

Controls of mantle source and condition of melt extraction on generation of the picritic lavas from the Emeishan large igneous province, SW China

Song-Yue Yu^{a,*}, Lie-Meng Chen^a, Jiang-Bo Lan^{a,*}, Yong-Sheng He^b, Qi Chen^{a,c}, Xie-Yan Song^a

^a State Key Laboratory of Ore Deposit Geochemistry, Institute of Geochemistry, Chinese Academy of Sciences, Guiyang 550081, China

^b State Key Laboratory of Geological Processes and Mineral Resources, China University of Geosciences, Beijing 100083, China

^c University of Chinese Academy of Sciences, Beijing 100049, China



ARTICLE INFO

Keywords:

ELIP
Picrite
Magnesium isotope
Primary magma
Mantle potential temperature
Melting condition

ABSTRACT

Like many continental flood basalt (CFB) provinces in the world, the source mantle compositions and melting conditions for generation of the Emeishan CFB are highly debated. We have carried out an integrated Sr-Nd-O-Mg isotopic study of the Emeishan picritic lavas to evaluate possible effects of mantle heterogeneity on the magma composition. Moreover, we have used PRIMELT3 (Herzberg and Asimow, 2015) to calculate the primary magma compositions and melting conditions for these picritic lavas. Picrites from Maoniuping, Tanglanghe and Wuguijing exhibit depleted Sr-Nd isotopic compositions ($^{87}\text{Sr}/^{86}\text{Sr}_\text{i} = 0.7038\text{--}0.7050$; $\varepsilon_{\text{Nd}} = 0.27\text{--}3.89$), normal mantle-like $\delta^{26}\text{Mg}$ (-0.27 to $-0.2\text{\textperthousand}$) and $\delta^{18}\text{O}$ ($5.0\text{--}5.4\text{\textperthousand}$), which can be explained by partial melting of plume materials with negligible contribution of sedimentary carbonates. The Wulongba picrites are characterized by depleted Sr-Nd isotopic compositions ($^{87}\text{Sr}/^{86}\text{Sr}_\text{i} = 0.7041\text{--}0.7045$; $\varepsilon_{\text{Nd}} = 2.57\text{--}2.85$), slightly lower $\delta^{26}\text{Mg}$ (-0.36 to $-0.23\text{\textperthousand}$) and higher $\delta^{18}\text{O}$ ($5.6\text{--}5.7\text{\textperthousand}$), which were attributed to involvement of minor sedimentary carbonates (magnesite) in their mantle source. The calculated mantle potential temperatures for the Emeishan picrites range from 1516 to 1596 °C. The initial melting pressures range from 4 to 5 GPa. The final melting pressures for the Wulongba picrites (2–3 GPa) are lower than those for the Tanglanghe, Maoniuping and Wuguijing picrites (> 3 GPa). This suggests that the Wulongba picrites were generated in shallower garnet-spinel transition zone of the upper mantle. Picrites from other three localities are entirely generated in garnet stability field of the upper mantle.

1. Introduction

It is generally believed that the voluminous lavas in typical flood basalt provinces reflect decompressional melting of the associated mantle plume, whereas a small volume of lithospheric mantle derived magma may be produced when the lithosphere is heated by the mantle plume (e.g. White and McKenzie, 1995; Arndt and Christensen, 1992). The geochemistry of continental flood basalts can provide valuable information on the nature of the mantle sources from which they were derived and on the extent of plume–lithosphere interaction (e.g., Arndt and Christensen, 1992). However, most flood basalts are highly evolved and variably contaminated by crustal materials when magma ascends to the surface (e.g., Arndt et al., 1993; Baker et al., 2000). In this regard, picritic lavas ($\text{MgO} > 12 \text{ wt\%}$, Le Bas, 2000) associated with flood basalts provide the best possibility of evaluating primitive magmas, which were parental to the more voluminous basaltic rocks (e.g., Norman and Garcia, 1999). In addition, variations in the pressures and

temperatures of partial melting also have a significant impact on magma composition (Klein and Langmuir, 1987; Kinzler and Grove, 1992, Kinzler, 1997). The nature and degree of mantle heterogeneity cannot be fully ascertained until such effects are evaluated (e.g., Putirka, 1999).

Primary magma composition, temperature and pressure of melting and melt fraction can now be quantitatively evaluated using PRIMELT3 software (Herzberg and Asimow, 2008, 2015). The PRIMELT3 software is calibrated from experiments on fertile peridotite (KR-4003, Walter, 1998) and parameterizations of these and other experimental results (Herzberg and O'Hara, 2002; Herzberg, 2004, 2006). It is a mass balance solution to the primary magma problem for a hypothetical peridotite mantle source. It uniquely constrains the primary magma composition corresponding to a given evolved magma by calculating a melt fraction that is common to both partial melts of mantle peridotite and to the primitive melts from which the magma was derived. It is thus different from other traditional methods of using olivine composition to

* Corresponding authors.

E-mail addresses: yusongyue@mail.gyig.ac.cn (S.-Y. Yu), lanjiangbo@mail.gyig.ac.cn (J.-B. Lan).

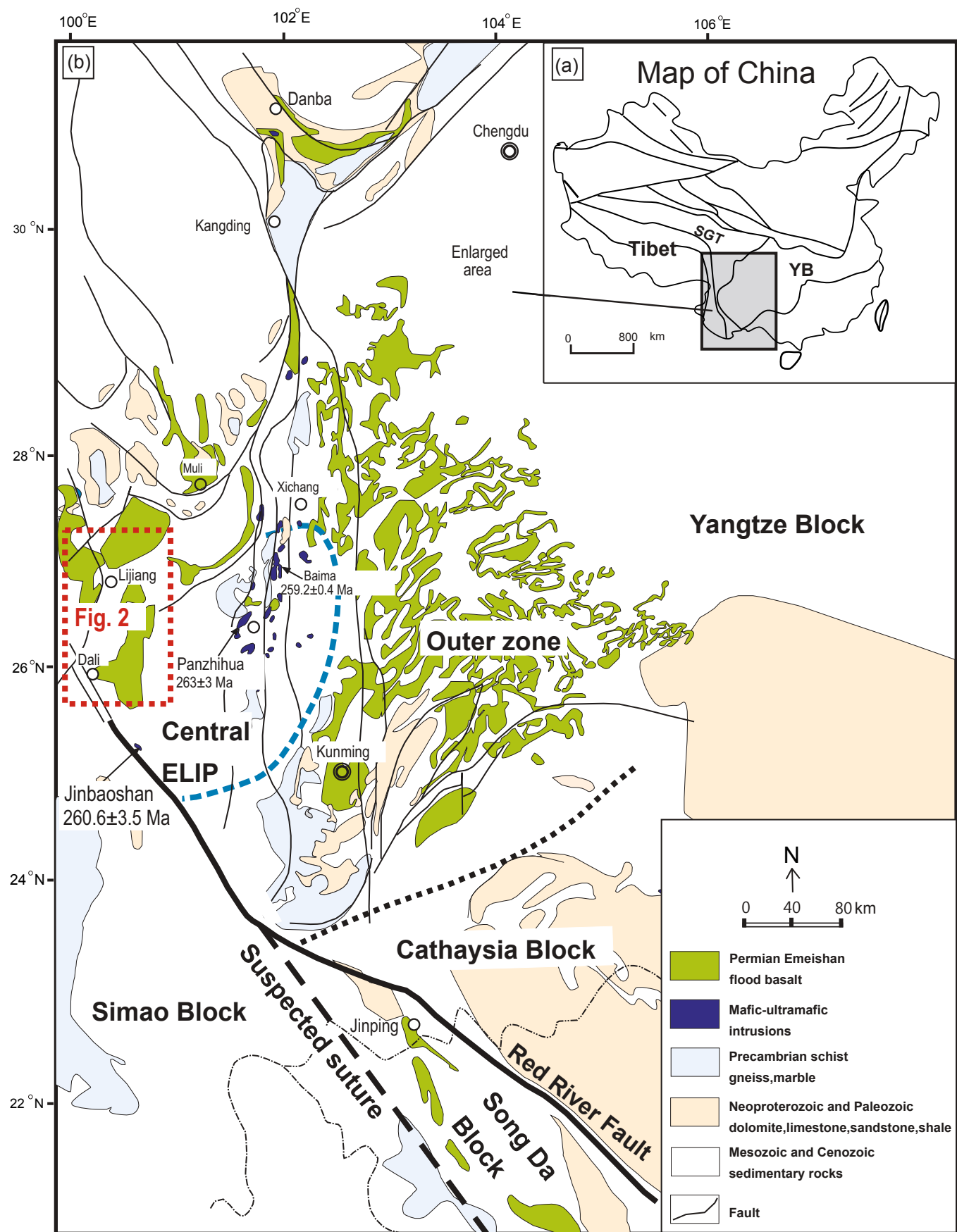


Fig. 1. Geologic map showing the simplified tectonic framework of China (a). Distribution of the late-Permian Emeishan flood basalts and coeval mafic intrusions (b, modified after Song et al., (2008b) and Li et al., (2016)).

constrain the primary magma composition (e.g., Courtier et al., 2007; Putirka et al., 2007; Putirka, 2008).

The Emeishan picritic lavas occur in the inner zone of the ELIP (Fig. 1). These highly magnesian volcanic rocks typically contain abundant olivine crystals and minor augite and chromite (e.g., Hanski et al., 2004; Zhang et al., 2006; Li et al., 2010, 2012; Kamenetsky et al., 2012; Yu et al., 2017; Ren et al., 2017; Wu et al., 2018). Picritic lavas from the ELIP have been divided into high-Ti ($Ti/Y = 800$) and low-Ti ($Ti/Y = 300$) end-members, with intermediate-Ti series that occur widely across the ELIP and form a continuous spectrum between the two end-members (Kamenetsky et al., 2012; Ren et al., 2017; Fig. S1). Melting conditions of the Emeishan picrites have been evaluated by many researchers (e.g., Zhang et al., 2006, 2019; Li et al., 2012). For example, using the equation from Herzberg and O'Hara (2002), the initial melting temperature and pressure for the Lijiang picrites are estimated to be 1630–1690 °C and 4.2–5.0 Gpa, respectively (Zhang et al., 2006). Employing the equation of Herzberg and Gazel (2009), the mantle potential temperature for the Daying picrites is estimated to be 1590 °C. Using trace element modeling, Zhang et al., (2019) estimated that the high-Ti primary melts are produced by variable degrees of mixing between a 10% partial melt formed at 3 GPa and a 4% partial melt formed at 7 GPa, whereas low-Ti melts were generated by 40% partial melting of a depleted mantle source at 3 GPa. Therefore, these researchers have come to different conclusions using different methods. To avoid this problem, it would be best to estimate the melting pressure and temperature for picritic lavas from different locations using a common method.

The source mantle compositions and lithology for the Emeishan lavas are still highly debated. Many researchers suggested that the high-Ti lavas are the products of deep melting of the mantle plume and that the low-Ti lavas were generated by shallow melting of the plume source materials plus the overlying lithospheric mantle (Xu et al., 2001; Xiao et al., 2004; He et al., 2010; Yu et al., 2017; Yao et al., 2019). Some researchers considered that both the high- and low-Ti lavas were derived from a hybridized mantle source consisting of peridotitic mantle and recycled oceanic crustal materials (Ren et al., 2017; Zhang et al., 2019; Yang and Liu, 2019). Kamenetsky et al., (2012) suggested that the low-Ti melts were derived from a peridotitic mantle, whereas the high-Ti melts were generated from a pyroxenite-rich mantle source. Zhang et al., (2008) considered that no clear evidence for recycled crustal materials in the mantle source of the Emeishan picrites. Therefore, the researchers have not reached consensus on source mantle composition and lithology for the Emeishan lavas.

In this study, picritic samples are collected from four locations (Wulongba, Wuguijing, Tanglanghe and Maoniuping) in the Dali-Lijiang area (Fig. 2). These samples plot between high-Ti and low-Ti endmembers and belong to intermediate-Ti series (Fig. S1). The range of $\delta^{18}\text{O}$ values for primitive olivine in these picritic samples is from 5.0 to 5.7‰, larger than the range of mantle olivine (4.8–5.4‰) (Yu et al., 2017). In order to better constrain the possible causes of such compositional differences, we have conducted an integrated Sr-Nd-O-Mg isotopic study of the picritic lavas from these four localities. We consider that limited sedimentary carbonates were involved in the genesis of the Emeishan picrites. Moreover, we have used PRIMELT3 software (Herzberg and Asimow, 2015) to calculate the primary magma compositions and melting conditions for generation of these picritic lavas. Such an approach can better constrain melting pressure and temperature for the Emeishan picritic lavas.

2. Geological background and sample description

The Permian Emeishan large igneous province is located in the western margin of the Yangtze Block, and is predominantly composed of mafic rocks including voluminous flood basalts and a large number of contemporaneous mafic-ultramafic intrusions (Fig. 1, e.g., Xu et al., 2001; Zhou et al., 2008). There are also minor felsic lavas and plutonic

rocks that form one endmember of the bimodal suite (e.g., Shellnutt and Zhou, 2007; Xu et al., 2010; Hei et al., 2018). These felsic rocks are genetically related to crustal melting or fractional crystallization of basaltic magma (Xu et al., 2010; Hei et al., 2018). The Emeishan flood basalts are exposed in a rhombic region of more than $2.5 \times 10^5 \text{ km}^2$ within Yunnan, Sichuan and Guizhou Provinces (Chung and Jahn, 1995; Xu et al., 2001; Song et al., 2001). They lie unconformably on limestones of the Early Late Permian Maokou Formation and are overlain unconformably by sediments belonging to the uppermost Permian Longtan Formation or Triassic sediments (He et al., 2003). The Emeishan volcanic succession is mainly composed of basaltic lavas with thicknesses ranging from several hundred meters in the east (Guizhou) to more than 5000 m in the west (Yunnan) (Xu et al., 2001; Song et al., 2001; Xiao et al., 2004; Ali et al., 2005). To date picritic lava flows have been found in the west (Dali, Binchuan, Lijiang, Yongsheng, Muli and Ertan) and in the south (Jinping-Songda) of ELIP. The picritic lava flows occur at various stratigraphic levels. The thicknesses of individual lava flows vary from ~3 to 50 m (Xiao et al., 2004; Zhang et al., 2006, 2008; Li et al., 2010, 2012). The associated mafic-ultramafic intrusions are exposed in the central zone of the ELIP because of severe post-eruptive uplift and erosion. Some of the large layered intrusions host important Fe-Ti-V oxide ore deposits whereas many relatively small intrusions may contain economic or uneconomic sulfides (e.g., Zhou et al., 2008; Song et al., 2008a).

The picrite samples used in this study are from Wulongba, Wuguijing, Tanglanghe and Maoniuping in the Dali-Lijiang region. Detailed sample information, including locality, petrography and trace element and oxygen isotope compositions of olivine phenocrysts have been presented in Yu et al., (2017) and Yao et al., (2019). Only a brief description is given below. The picrite samples contain ~20–35% olivine grains and minor augite phenocrysts (< 1%). Some olivine phenocrysts contain chromite inclusions. The fine-grained groundmass consists of pyroxene, plagioclase and minor Fe-Ti oxides. The Emeishan picrites have MgO contents ranging from 14 to 26 wt%. Most samples exhibit typical OIB-like trace element patterns (Fig. S2). The range of $\delta^{18}\text{O}$ values for primitive olivine in these picritic samples is from 5.0 to 5.7‰, larger than that of mantle olivine (4.8–5.4‰) (Yu et al., 2017). Olivine phenocrysts from the Wulongba picrites have lower Ti, Cr and higher Al concentrations than those from the Maoniuping, Tanglanghe and Wuguijing picrites (Yao et al., 2019).

3. Analytical methods

The chemical compositions of olivine phenocrysts were determined by a CAMECA SX50 electron microprobe in the Department of Geological Sciences, Indiana University. Major elements in olivine were analyzed using an accelerating voltage of 15 kev, a beam current of 20 nA, a beam size of 1 μm and a peak counting time of 20 s. Analytical conditions for minor elements (Ca, Mn and Ni) were 100 nA beam current and peak counting time of 100 s. Under these conditions, the detection limits are 20 ppm Ca, 64 ppm Mn and 99 ppm Ni. Mineral standards were used to monitor the accuracy of the analyses, and analytical uncertainty was within ± 2% of the accepted values. Analytical results are presented in Table S1.

Sr-Nd isotope analyses were carried out at the Radiogenic Isotope Facility, School of Earth Science, the University of Queensland. About 50 mg of rock powders were dissolved in distilled HF-HNO₃ Savillek screwtop Teflon beakers at 185 °C for 3 days. Sr, Nd chemical separations followed an improved procedure described by Pin and Zalduegui (1997), Deniel and Pin (2001) and Miková and Denková (2007). Sr was separated from other elements by Sr-Spec resin and deposited on Ta filaments with TaF₅. Isotope ratios were analyzed on a VG Sector 54 thermal ionization mass spectrometer (TIMS). As a monitor of the detector efficiency drift of the instrument, the NBS-987 standard was measured repeatedly during analysis of the samples and yielded an average of 0.710224 ± 18 (2σ, n = 42). The data were corrected using

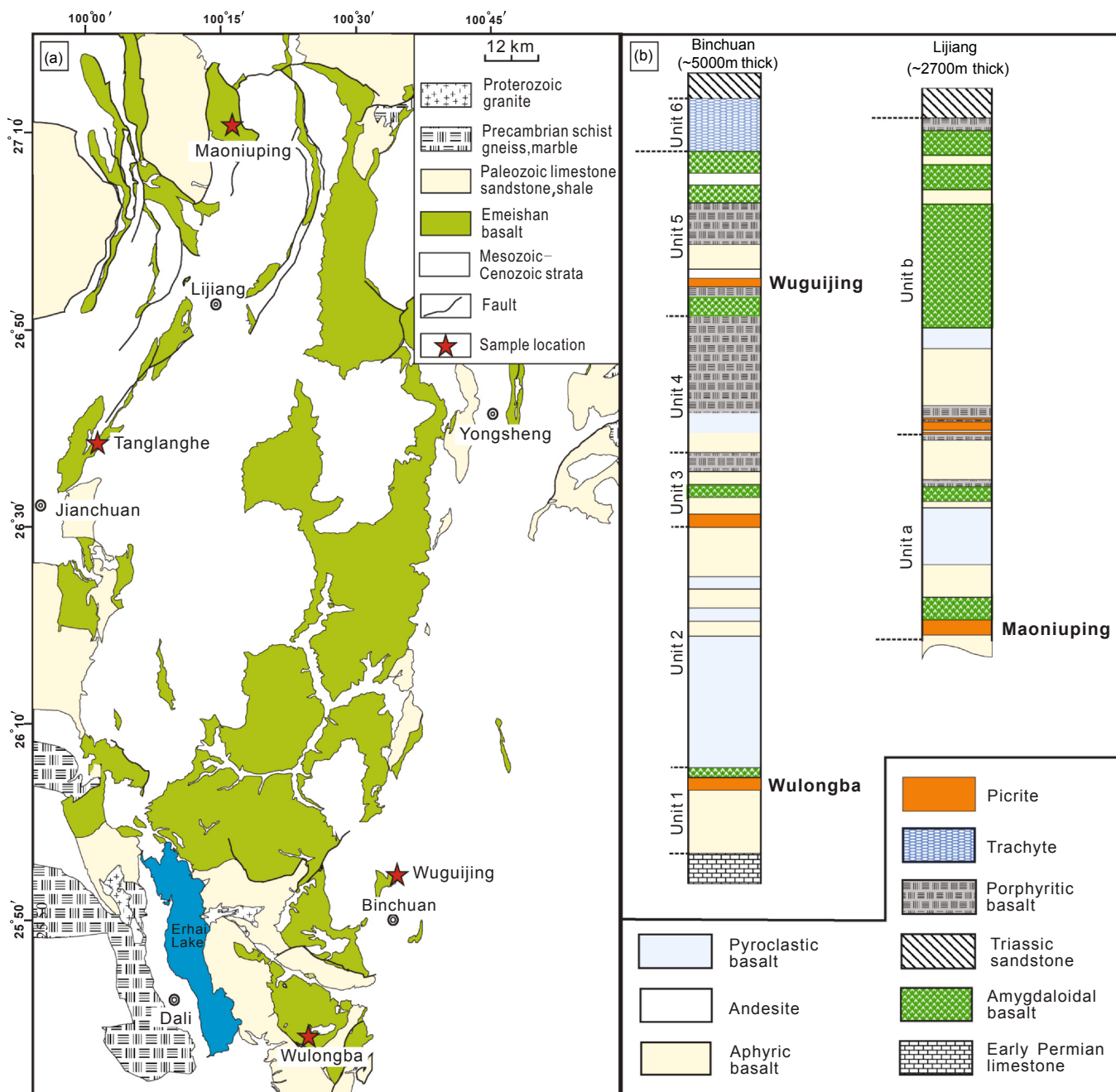


Fig. 2. Distribution of the Emeishan flood basalts in the studied area (a, after Yunnan, 1990). Stratigraphic columns at Binchuan and Lijiang area (b, modified after Xiao et al., 2004; Zhang et al., 2006).

the deviation of this mean value from the laboratory's previously obtained long-term average of 0.710249 ± 28 (2σ). Separation of Nd from the REE fractions was carried out using Ln-Spec resin. Isotope ratios were determined on a Nu Plasma multi-collector inductively coupled plasma mass spectrometer (MC-ICPMS). Mass fractionation and instrumental bias were calibrated by normalizing raw ratios to $^{146}\text{Nd}/^{144}\text{Nd}$ of 0.7219. Accuracy was examined by analyzing the JNd-1, BHVO-2 and BCR-2 USGS rock standards. The JNd-1 standard gave $^{143}\text{Nd}/^{144}\text{Nd} = 0.512114 \pm 8$ (2σ , $n = 10$), consistent with the recommended value (0.512115 ± 7 , Tanaka et al., 2000). The BHVO-2 gave $^{143}\text{Nd}/^{144}\text{Nd} = 0.512982 \pm 6$ (2σ , $n = 3$), consistent with the expected value of 0.512979 ± 14 , and BCR-2 standard gave $^{143}\text{Nd}/^{144}\text{Nd} = 0.512631 \pm 5$ (2σ , $n = 4$), matching the certified value of 0.512635 ± 29 (GeoReM: <http://georem.mpch-mainz.gwdg.de/>). Analytical results are shown in Table 1.

Mg isotopic analysis was carried out at the State Key Laboratory of Geological Processes and Mineral Resources, China University of Geosciences, Beijing, following analytical procedures described by Teng et al., (2007) and Ke et al., (2016). For each sample, approximately 2–4 mg whole-rock powders were digested in the screw-top beakers with a mixture of HF and HNO₃ (3:1). Then, they were heated to dryness at 70°C. The products were dissolved into a mixture of HCl and HNO₃ (3:1), evaporated to dryness and dissolved into HNO₃ to reach complete dissolution. Mg was purified using the ion exchange resin AG50W-X8 (Bio-Rad 200–400 mesh) in a 1 N HNO₃ medium following the procedure described by Teng et al., (2007) and Ke et al., (2016). The same column procedure was processed twice to gain a pure Mg solution. Isotope ratios were determined on a Neptune plus MC-ICP-MS with a 'wet' sample introduction system. The analysis for each sample was repeated 4–6 times in order to attain a better reproducibility and

Table 1

Whole-rock Sr-Nd isotopic compositions of the Emeishan picrites.

Sample	Location	$(^{87}\text{Sr}/^{86}\text{Sr})_0 \pm 2\sigma$	$(^{143}\text{Nd}/^{144}\text{Nd})_0 \pm 2\sigma$	$(^{87}\text{Sr}/^{86}\text{Sr})_t^{**}$	$(^{143}\text{Nd}/^{144}\text{Nd})_t^{**}$	$\epsilon\text{Nd}(t)^{**}$
YY13-09	Wulongba	0.705446 \pm 8	0.512761 \pm 5	0.704222	0.512439	2.79
YY13-10		0.705441 \pm 7	0.512758 \pm 5	0.704307	0.512437	2.74
YY13-11		0.705445 \pm 7	0.512762 \pm 5	0.704216	0.512443	2.85
YY13-105		0.705371 \pm 7	0.512762 \pm 5	0.704370	0.512438	2.77
YY13-106		0.705523 \pm 8	0.512751 \pm 5	0.704130	0.512428	2.57
YY13-108		0.705452 \pm 8	0.512762 \pm 5	0.704476	0.512433	2.67
YY13-109	Tanglanghe	0.704635 \pm 8	0.512715 \pm 5	0.703967	0.512491	3.81
YY13-110		0.704428 \pm 10	0.512724 \pm 5	0.703853	0.512494	3.86
YY13-111		0.704619 \pm 8	0.512724 \pm 4	0.704176	0.512493	3.83
YY13-113		0.704505 \pm 7	0.512726 \pm 5	0.703772	0.512496	3.89
YY13-117	Maoniuping	0.705578 \pm 8	0.512506 \pm 4	0.704803	0.512329	0.63
YY13-118		0.705556 \pm 8	0.512509 \pm 4	0.704750	0.512322	0.50
YY13-119		0.704469 \pm 8	0.512718 \pm 5	0.704139	0.512488	3.73
YY13-121		0.705543 \pm 8	0.512512 \pm 5	0.704717	0.512321	0.49
DL15-42		0.704512 \pm 37		0.703410		
DL15-50		0.704713 \pm 23	0.512705 \pm 6	0.704086	0.512459	3.18
DL15-16	Wuguiqing	0.705599 \pm 10	0.512583 \pm 6	0.704958	0.512364	1.32
DL15-20		0.705555 \pm 10	0.512582 \pm 6	0.704815	0.512361	1.27
DL15-23		0.705881 \pm 16	0.512538 \pm 5	0.704801	0.512310	0.27

** Measured Sr-Nd isotope ratios (subscript 0) are age-corrected (t) to 260 Ma.

Table 2

Magnesium isotopic compositions of the Emeishan picrites as well as standard reference materials.

Sample	Location	$\delta^{25}\text{Mg} (\text{\textperthousand})$	2SD	$\delta^{26}\text{Mg} (\text{\textperthousand})$	2SD	Note
YY13-09	Wulongba	-0.18	0.06	-0.36	0.03	
YY13-09 (Duplicate)		-0.18	0.02	-0.31	0.05	
YY13-10		-0.14	0.03	-0.28	0.02	
YY13-11		-0.14	0.02	-0.28	0.04	
YY13-105		-0.15	0.02	-0.27	0.04	
YY13-106		-0.15	0.03	-0.27	0.03	
YY13-108		-0.11	0.02	-0.23	0.03	
YY13-109	Tanglanghe	-0.13	0.04	-0.27	0.04	
YY13-110		-0.13	0.02	-0.25	0.02	
YY13-111		-0.13	0.02	-0.25	0.04	
YY13-113		-0.11	0.03	-0.21	0.03	
YY13-114		0.09	0.05	0.18	0.02	
YY13-114 (Duplicate)		0.12	0.05	0.20	0.01	
YY13-117	Maoniuping	-0.14	0.04	-0.26	0.05	
YY13-118		-0.13	0.04	-0.27	0.01	
YY13-119		-0.11	0.03	-0.27	0.07	
YY13-121		-0.12	0.03	-0.26	0.02	
DL15-42		-0.10	0.02	-0.22	0.02	
DL15-50		-0.09	0.02	-0.22	0.09	
DL15-52		-0.14	0.02	-0.26	0.05	
DL15-53		-0.08	0.02	-0.19	0.05	
DL15-16	Wuguijing	-0.12	0.04	-0.24	0.03	
DL15-20		-0.12	0.04	-0.20	0.05	
DL15-21		-0.13	0.03	-0.27	0.02	
DL15-22		-0.14	0.03	-0.25	0.03	
DL15-23		-0.12	0.06	-0.23	0.07	
DL15-24		-0.08	0.02	-0.19	0.04	
DL15-24 (Duplicate)		-0.11	0.06	-0.20	0.05	
DL15-25		-0.10	0.03	-0.21	0.03	
BHVO-2	Standard	-0.10	0.05	-0.21	0.05	This study
BHVO-2*		-0.10	0.04	-0.20	0.07	Recommended value
BCR-2		-0.06	0.04	-0.13	0.05	This study
BCR-2**		-0.08	0.02	-0.16	0.01	Recommended value

* After Teng et al., (2015); ** After An et al., (2014); ***

accuracy. Mg isotopic ratios are reported in δ -notation relative to the international standard DSM3: $\delta^X\text{Mg} (\text{\textperthousand}) = 1000 \times ((^{29}\text{Mg}/^{24}\text{Mg})_{\text{sample}} / (^{29}\text{Mg}/^{24}\text{Mg})_{\text{DSM3}} - 1)$, where X refers to mass 25 or 26. The long-term external precision is ± 0.06 (2SD) (Ke et al., 2016). Data qualities were monitored by two USGS rock standards (BHVO-2 and BCR-2), which were processed as unknown samples in the same chemical and

analytical procedures. The blank was 7 ng for Mg. Analytical results are shown in Table 2.

4. Results

4.1. Olivine compositions

The chemical compositions of olivine phenocrysts in the picrite samples from Wulongba, Tanglanghe, Maoniuping and Wuguijing are given in Table S1. It is noted that chemical compositions of primitive olivine cores ($Fo > 88$) have been reported in Yu et al., (2017). The analytical results in this study are chemical compositions of olivine rims and olivine phenocrysts with low Fo (< 88). In thin sections olivine phenocrysts vary from $< 20 \mu\text{m}$ to $> 2 \text{ mm}$. Most large olivine phenocrysts are normally zoned, with core-rim Fo contents varying up to 7 mol% (Table S1). Fo contents of olivine rim range from 84 to 87 at Wulongba, 83 to 85 at Tanglanghe, and 85 to 87 at Maoniuping. Significant compositional zoning is not observed in small grains with diameters $< 20 \mu\text{m}$ across. The Fo contents of such small grains are similar to the rim of larger grains in a given sample. In general, olivine phenocrysts from the Emeishan picrites exhibit highly variable compositions. Fo contents of Olivine phenocrysts vary from 81.3 to 92.8 at Wulongba, 79.5–90.9 at Wuguijing, 80.6–90.7 at Tanglanghe and 81.2–90.5 at Maoniuping. Olivine phenocrysts with high Fo contents ($Fo > 90$) are more abundant at Wulongba compared to those at Tanglanghe, Maoniuping and Wuguijing. Olivine phenocrysts in the Emeishan picrites are characterized by a positive Ni- Fo correlation (Fig. 3a) and variable Ca contents from 1400 to 3600 ppm with no correlation with Fo contents (Fig. 3b). The concentrations of Ca in olivines from the Emeishan picrites are significantly higher than that of mantle olivine ($< 1000 \text{ ppm Ca}$, e.g., Yu et al., 2009). The zoning patterns and compositional variations of olivine phenocrysts in the picrites from Wulongba, Tanglanghe, Maoniuping and Wuguijing are remarkable similar to those from elsewhere in the ELIP reported previously by Hanski et al., (2010) and Li et al., (2012).

4.2. Sr-Nd-Mg isotopes

Sr-Nd isotopic ratios were back-calculated to their initial values at 260 Ma and listed in Table 1 and illustrated in Fig. 4. The ε_{Nd} values range from 2.57 to 2.85 for the Wulongba samples, from 3.81 to 3.89 for the Tanglanghe samples, from 0.49 to 3.73 for the Maoniuping samples and from 0.27 to 1.32 for the Wuguijing samples. The $^{87}\text{Sr}/^{86}\text{Sr}_i$ values vary from 0.7041 to 0.7045 for the Wulongba picrites, from 0.7037 to 0.7042 for the Tanglanghe picrites, from 0.7034 to 0.7048 for the Maoniuping samples and from 0.7048 to 0.7049 for the Wuguijing samples. There is no correlation between Nb/Th and ε_{Nd} , or between Th/Yb and $^{87}\text{Sr}/^{86}\text{Sr}_i$ (Fig. 5).

Mg isotopic data of the Emeishan picrites are listed in Table 2 and shown in Fig. 4b. The $\delta^{26}\text{Mg}$ values of the Wulongba picrites vary from -0.36 to $-0.23\text{\textperthousand}$ with an average of $-0.28 \pm 0.08\text{\textperthousand}$ (2SD, $n = 6$). The $\delta^{26}\text{Mg}$ values of the Maoniuping picrites vary from -0.27 to $-0.19\text{\textperthousand}$ with an average of $-0.25 \pm 0.06\text{\textperthousand}$ (2SD, $n = 8$). The Tanglanghe picrites have $\delta^{26}\text{Mg}$ values ranging from -0.27 to $-0.21\text{\textperthousand}$ with an average of $-0.25 \pm 0.04\text{\textperthousand}$ (2SD, $n = 4$). The Wuguijing picrites have $\delta^{26}\text{Mg}$ values ranging from -0.27 to $-0.19\text{\textperthousand}$ with an average of $-0.23 \pm 0.06\text{\textperthousand}$ (2SD, $n = 4$). Overall, the Emeishan picritic samples collected from Tanglanghe, Maoniuping and Wuguijing have identical Mg isotopic compositions, similar to the normal mantle value ($-0.25 \pm 0.04\text{\textperthousand}$, Teng, 2017). The Wulongba picrites have slightly lighter Mg isotopes compared with samples from other three locations. Moreover, the $\delta^{26}\text{Mg}$ values of the Emeishan picrites are similar to those of the Emeishan basalts from Dongchuan and Qiaojia (Tian et al., 2017). It is noted that $\delta^{26}\text{Mg}$ values of the Emeishan picrites and basalts are significantly higher than those of the igneous rocks (including basalts, mafic-ultramafic intrusions, nephelinites, kimberlites and carbonatites) from the Tarim large igneous province (-1.09 to $-0.28\text{\textperthousand}$, Cheng et al., 2017, 2018). The $\delta^{26}\text{Mg}$ values do not vary with increasing of MgO or Cr contents (Fig. 6).

5. Discussion

5.1. Crustal contamination and mantle heterogeneity

Variable degrees of crustal contamination are generally anticipated for mantle-derived magmas migrating through continental crust to the surface (Carlson, 1991; Hawkesworth et al., 1984; Hergt et al., 1991). Crustal materials commonly have much lower Nb/Th and ε_{Nd} ratios, and much higher Th/Yb and $^{87}\text{Sr}/^{86}\text{Sr}_i$ values than uncontaminated mantle-derived magmas. Relatively high Nb/Th (7–11) and ε_{Nd} (0.3–3.8) and low $^{87}\text{Sr}/^{86}\text{Sr}_i$ (0.703–0.705) for the picritic samples in this study indicate that they were little affected by crustal contamination. Moreover, positive correlations are expected in the diagrams of Nb/Th versus ε_{Nd} and Th/Yb versus $^{87}\text{Sr}/^{86}\text{Sr}_i$ for a suite of rocks formed by magmas with variable degrees of crustal contamination. However, no regular correlation is observed in these diagrams for the Emeishan picrites (Fig. 5), suggesting insignificant crustal contamination. Moreover, insignificant crustal contamination in the Emeishan picrites also gains supporting evidence of the lack of negative Nb, Ta, and Ti anomalies in the primitive mantle-normalized spiderdiagram (Fig. S2), which are the characteristics of continental crust (Rudnick and Fountain, 1995). The lack of correlation between ε_{Nd} and SiO₂ (not shown) is also consistent with negligible crustal assimilation for the

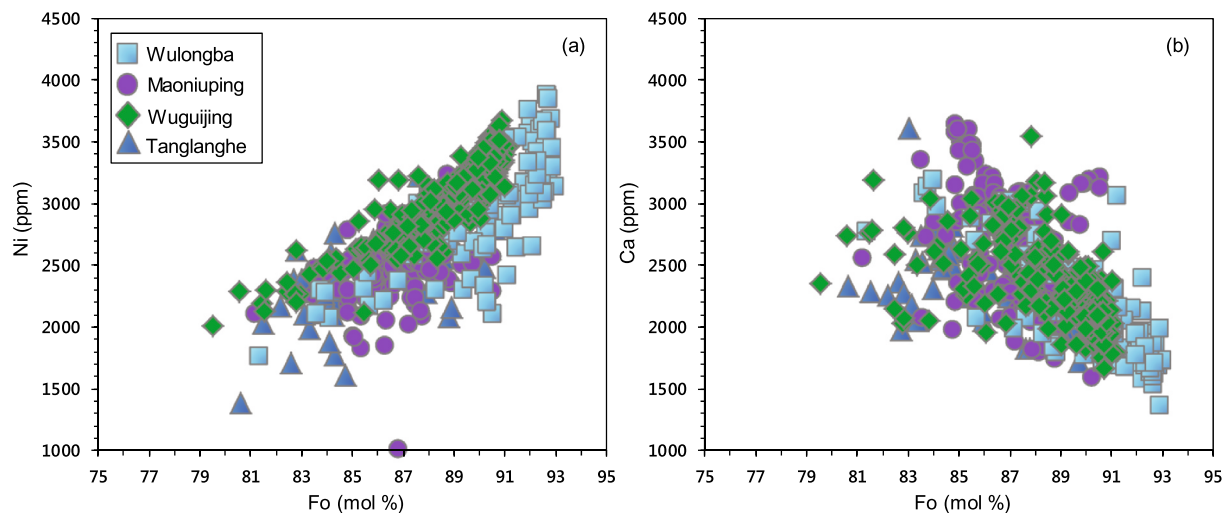


Fig. 3. Chemical compositions of olivine phenocrysts from the Emeishan picrites. Plot of Fo versus Ni and Ca (a-b).

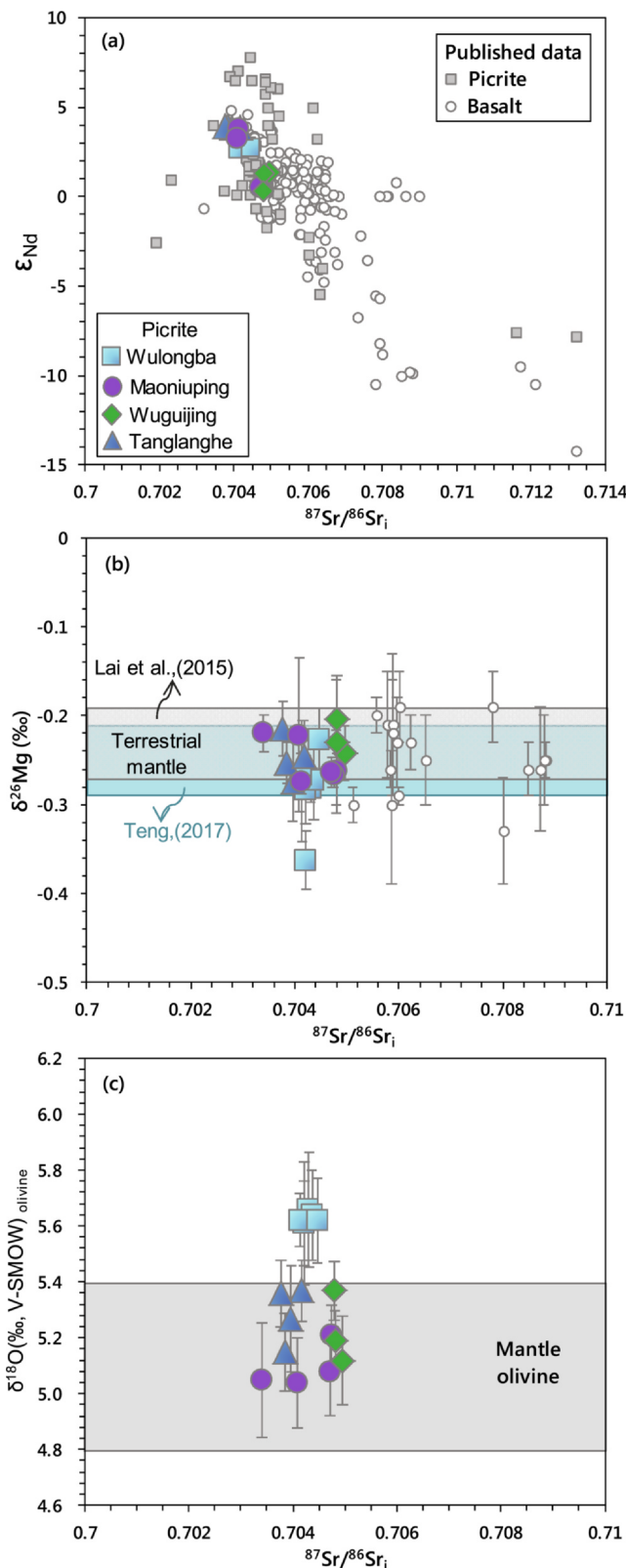


Fig. 4. Sr-Nd-Mg-O isotopic compositions of the Emeishan picrites. (a) $^{87}\text{Sr}/^{86}\text{Sr}_i$ versus ϵ_{Nd} . (b) $^{87}\text{Sr}/^{86}\text{Sr}_i$ versus $\delta^{26}\text{Mg}$. Sr-Nd-Mg isotopic compositions of the Emeishan basalts from Tian et al., (2017) are also shown for comparison. Oxygen isotopic compositions of the Emeishan picrites are from Yu et al., (2017). Other published data of the Emeishan picrites and basalts are from Geochemical Rock Database <http://georoc.mpch-mainz.gwdg.de/georoc/>. The gray and light green bands represent recommended $\delta^{26}\text{Mg}$ values of the terrestrial mantle from Lai et al., (2015) and Teng, (2017), respectively. (c) $^{87}\text{Sr}/^{86}\text{Sr}_i$ versus $\delta^{18}\text{O}$. Oxygen isotope compositions of mantle olivine (4.8–5.4‰) are after Mattey et al., (1994). (For interpretation of the references to colour in this figure legend, the reader is referred to the web version of this article.)

ascent of magma to the surface, constrained by the commonly presence of a large number of Mg-rich olivine phenocrysts in those volcanic rock samples (Yu et al., 2017). We thus believe that, although minor crustal contamination may occur, it was certainly not an important factor controlling the chemical variations of the Emeishan picrites.

Picrites from Maoniuping, Tanglanghe and Wuguijing exhibit typical OIB-like trace element patterns (Fig. S2), high ϵ_{Nd} and low $^{87}\text{Sr}/^{86}\text{Sr}_i$ values (Fig. 4a), which are similar to the high-Ti basalts in the ELIP, indicating origin from partial melting of a mantle plume (e.g., Chung and Jahn, 1995; Xu et al., 2001; Xiao et al., 2004; Zhang et al., 2006). Moreover, primitive olivine phenocrysts from these picrites display normal mantle-like $\delta^{18}\text{O}$ values (Fig. 4c, Yu et al., 2017), which suggests that the plume source materials are characterized by a “normal” oxygen isotope signature. In contrast, the Wulongba picrites display flat trace element patterns without positive Nb or Ta anomaly, which is the typical character of OIB (Fig. S2). This indicates that they are not the typical melts of a mantle plume. Furthermore, primitive olivine phenocrysts from the Wulongba picrites display abnormally high $\delta^{18}\text{O}$ values (Fig. 4c), which was attributed to have originated from subduction-modified lithospheric mantle (Yu et al., 2017). The Wulongba picrites have high ϵ_{Nd} and low $^{87}\text{Sr}/^{86}\text{Sr}_i$ values, similar to those from Maoniuping, Tanglanghe and Wuguijing (Fig. 4a). This suggests that the lithospheric mantle beneath the Dali-Binchuan region may also have depleted Sr-Nd isotopic compositions, which is indistinguishable from the plume source materials.

The $\delta^{26}\text{Mg}$ values of the Emeishan picrites vary from -0.36 to $-0.19\text{\textperthousand}$. There is no correlation between $\delta^{26}\text{Mg}$ and MgO for the picritic samples from each locality (Fig. 6a), which suggests that olivine fractionation or accumulation has little effect on Mg isotopic compositions of these picritic lavas. This speculation also gains supporting evidence from the previous Mg isotopic study of the Hawaii lavas by Teng et al., (2007). These researchers observed that the Kilauea Iki lavas from Hawaii with highly variable MgO (2.4–26.9 wt%) exhibit no resolvable variations in their Mg isotopic compositions, indicating the absence of detectable Mg isotope fractionation during basalt differentiation. Moreover, many other studies also suggested that fractional crystallization of olivine and pyroxene cause no detectable Mg isotope fractionation during basalt differentiation (Young et al., 2009; Huang et al., 2011; Liu et al., 2011; Schäuble, 2011; Su et al., 2017; Guo et al., 2019). Chromite is an early crystallization phase in basaltic magmas and is Mg-rich and isotopically heavier than silicate minerals ($\delta^{26}\text{Mg} = -0.1$ to $+0.4\text{\textperthousand}$, e.g., Su et al., 2017, 2019). Chromite crystallization or accumulation of chromite thus has the potential to modify Mg isotopic compositions of the mantle-derived magmas (Su et al., 2019). The Emeishan picritic samples have highly variable Cr contents (703–2560 ppm). If we assume the primary melts of the Emeishan picrites have similar Cr contents to those of experimental partial melts of mantle peridotite (2120–3760 ppm, e.g., Walter, 1998). Then only four samples with the highest Cr contents (2060–2560 ppm) can be regarded as near primary melts with negligible chromite crystallization. The other picritic samples with low Cr (< 2000 ppm) can be explained by fractional crystallization of chromite. However, the $\delta^{26}\text{Mg}$ values of these samples with low Cr contents are indistinguishable from

Emeishan picrites. Crustal materials commonly have lower ϵ_{Nd} and higher SiO₂ than uncontaminated mantle-derived magmas. Thus, negative correlation between ϵ_{Nd} and SiO₂ is expected by the assimilation-fractionation-crystallization (AFC) model (DePaolo, 1981). At last, limited interaction with crust is also suggested by speculated rapid

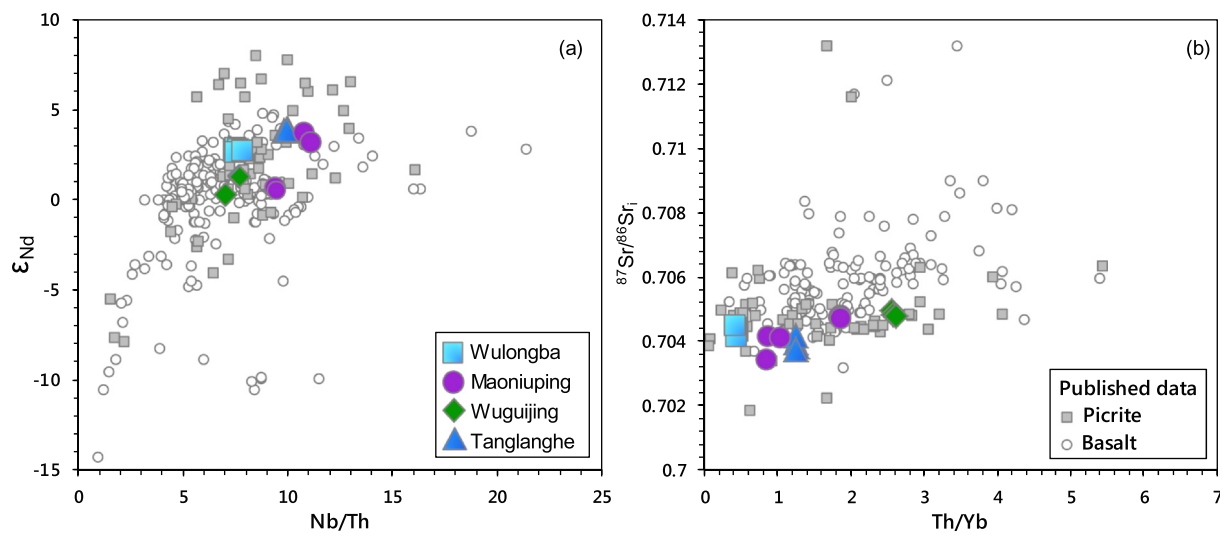


Fig. 5. Nb/Th versus ϵ_{Nd} (a), Th/Yb versus $^{87}\text{Sr}/^{86}\text{Sr}_i$ (b) for the Emeishan picrites. Data sources as in Fig. 4.

those samples with high Cr contents (Fig. 6b). There is no correlation between ^{82}Mg and Cr contents (Fig. 6b). All these features indicate that the effect of chromite fractionation on Mg isotopic compositions of the Emeishan picritic lavas is relatively small, which cannot be identified under the current analytical precision of Mg isotopes.

The picrites from Tanglanghe, Maoniuping and Wuguijing exhibit normal mantle-like $\delta^{26}\text{Mg}$ (-0.27 to $-0.20\text{\textperthousand}$) and $\delta^{18}\text{O}$ (5.0 – $5.4\text{\textperthousand}$), and depleted Sr isotopic compositions ($^{87}\text{Sr}/^{86}\text{Sr}_i = 0.7041$ – 0.7045). Such features can be well explained by partial melting of a carbonate-barren mantle source. Although high CaO/Al₂O₃ ratios (0.9–1.4) for these picritic samples can be regarded as an indicator of a carbonated mantle source, they also can be explained by high pressure ($> 4\text{GPa}$) melting of a volatile-free peridotitic mantle (e.g., Walter, 1998). Yu et al. (2017) suggested picrites from Maoniuping, Tanglanghe and Wuguijing are derived from partial melting of the Emeishan mantle plume. If this is true, it means that the Emeishan plume source materials are carbonate-barren, which is distinct from the Tarim mantle plume containing a large amount of recycled sedimentary carbonates (e.g., Cheng et al., 2017, 2018).

The Wulongba picrites have slightly lower $\delta^{26}\text{Mg}$ (-0.36 to $-0.23\text{\textperthousand}$) compared with picrites from Tanglanghe, Maoniuping and Wuguijing (-0.27 to $-0.19\text{\textperthousand}$). Marine carbonates typically have low

$\delta^{26}\text{Mg}$ ($-5.31\text{\textperthousand}$ to $-1.09\text{\textperthousand}$, Galy et al., 2002; Young and Galy, 2004; Tipper et al., 2006; Brenot et al., 2008; Pogge von Strandmann et al., 2008; Higgins and Schrag, 2010). Subduction would deliver altered oceanic crust along with marine sediments with distinct Mg isotopic compositions to the mantle. Moreover, sedimentary carbonates (including calcite and dolomite) are also characterized by high CaO, $^{87}\text{Sr}/^{86}\text{Sr}_i$ and $\delta^{18}\text{O}$ (Plank and Langmuir, 1998; Huang and Xiao, 2016). Slightly low $\delta^{26}\text{Mg}$ (-0.36 to $-0.23\text{\textperthousand}$) for the Wulongba samples may be attributed to involvement of minor sedimentary dolomites or calcites in their mantle source. Slightly high $\delta^{18}\text{O}$ values (5.6 – $5.7\text{\textperthousand}$) for the Wulongba samples are also consistent with partial melting of such a mantle source. However, the Wulongba picrites exhibit depleted Sr isotopic compositions ($^{87}\text{Sr}/^{86}\text{Sr}_i = 0.7041$ – 0.7045), which is inconsistent with involvement of sedimentary dolomite or calcite. The Wulongba samples also have lower CaO/Al₂O₃ (0.9–1.0) compared with those of partial melts of carbonated peridotite (1–1.7, e.g., Dasgupta et al., 2007). Such a decoupled geochemical feature may be explained by involvement of magnesite in the mantle source. During subduction, sedimentary calcite would react with orthopyroxene to form dolomite and diopside at pressures between 23 and 45 kbars (Kushiro, 1975). Beyond a pressure of 45 kbars, sedimentary calcite and dolomite would react with orthopyroxene to form magnesite and

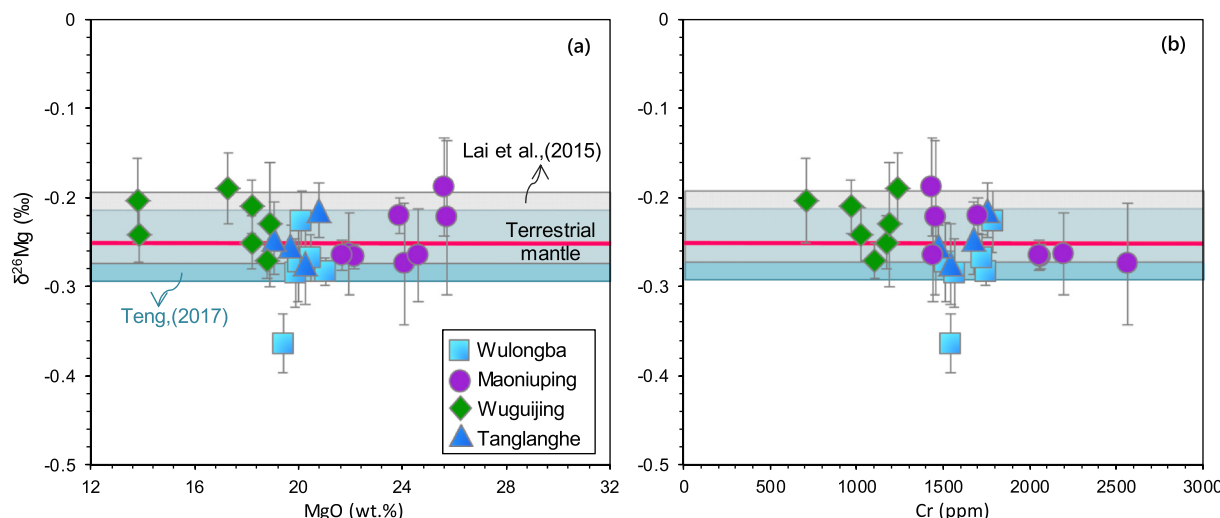


Fig. 6. Plots of $\delta^{26}\text{Mg}$ versus MgO and Cr contents for the Emeishan picrites. Data sources as in Fig. 4. The pink line represent the average $\delta^{26}\text{Mg}$ value of the normal mantle ($-0.25\text{\textperthousand}$, Teng et al., 2010). (For interpretation of the references to colour in this figure legend, the reader is referred to the web version of this article.)

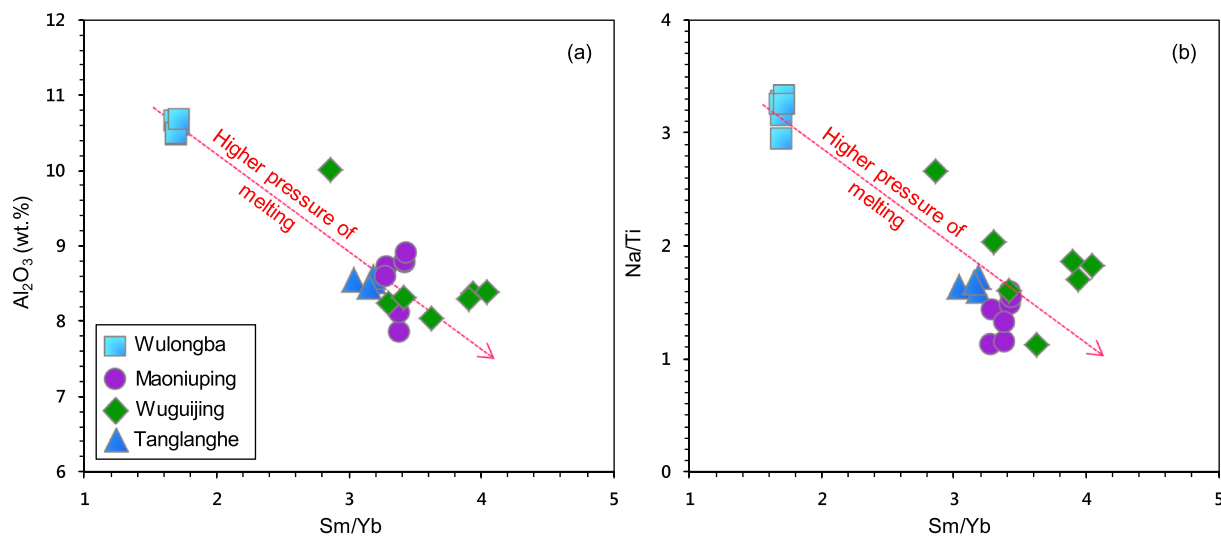


Fig. 7. Geochemical characteristics of primitive melts of the Emeishan picrites, (c) Sm/Yb verus Al₂O₃; (b) Sm/Yb verus Na/Ti (mole ratio). Primary melts of the Emeishan picrites are calculated using software PRIMELTS 3 from Herzberg and Asimow, (2015).

diopside (Kushiro, 1975). Magnesite, one of the products of the reaction, is expected to be poor in Ca and Sr since these two elements display similar chemical behavior and coexist through isomorphism (e.g., Depaolo, 1986; Cheng et al., 2017). Therefore, involvement of magnesite in the mantle source of the Wulongba picritic magmas will not significantly change their CaO/Al₂O₃ and ⁸⁷Sr/⁸⁶Sr_i values, but it has a great impact on their Mg-O isotopic compositions. As discussed earlier, the Emeishan plume source materials are carbonate-barren. Magnesite is thus unlikely from the mantle plume itself, but may be from the convective upper mantle or subduction-modified lithospheric mantle related to ancient subduction.

Mantle plume-related lavas display variable Mg isotopic compositions. For example, the $\delta^{26}\text{Mg}$ values for oceanic island basalts (OIBs) from Hawaii, Louisville, and Society island and Cook-Austral chain range from $-0.18\text{\textperthousand}$ to $-0.36\text{\textperthousand}$ (Teng et al., 2010; Zhong et al., 2017). In specific, alkaline OIBs from these four localities have slightly lower $\delta^{26}\text{Mg}$ ($-0.36\text{\textperthousand}$ to $-0.24\text{\textperthousand}$) than those of tholeiitic OIBs (-0.30 to $-0.18\text{\textperthousand}$), which was attributed to different degrees of partial melting of a garnet-bearing (peridotitic or pyroxenitic) source (Zhong et al., 2017). Moreover, OIBs from the Pitcairn and Rarotonga islands show low $\delta^{26}\text{Mg}$ (-0.40 to $-0.25\text{\textperthousand}$), which was considered to be derived from a plume source containing recycled ancient "ghost" carbonates (Wang et al., 2018). Basalts and magmatic carbonatites from the Tarim large igneous province also display low $\delta^{26}\text{Mg}$ values (-0.45 to $-0.29\text{\textperthousand}$ and -1.09 to $-0.85\text{\textperthousand}$, respectively), which was suggested to be derived from a plume source containing magnesite or periclase/perovskite (Cheng et al., 2017, 2018). In general, OIBs and the Tarim lavas were derived from mantle plume sources containing variable amounts of carbonates. Some mantle plumes are carbonate-barren, such as Hawaii, Louisville, and Society island and Cook-Austral chain. Others contain recycled carbonates, such as Pitcairn, Rarotonga and Tarim. As stated earlier, we speculated that Emeishan plume should be carbonate-barren and display normal mantle-like $\delta^{26}\text{Mg}$. The Wulongba picrites with slightly low $\delta^{26}\text{Mg}$ values were considered to be derived from the convective upper mantle or subduction-modified lithospheric mantle containing minor magnesite.

5.2. Calculation of the Emeishan primary magma compositions

The model PRIMELT3 has been used here to calculate primary magma compositions from the major element compositions of the Emeishan picrites. The Emeishan picritic samples in this study did not show evidence of early augite crystallization based on covariation

between MgO and CaO (Fig. S1b). This is also supported by lack of augite phenocryst in these samples (Yu et al., 2017). Moreover, melts derived from pyroxenite sources can be identified according to their deficiency in CaO for a given MgO content compared with melts from mantle peridotite (Fig. S1b). Such samples from Emeishan can also be identified using the PRIMELT3 software, and filtered accordingly. Reverse-modeling involves the incremental addition or subtraction of equilibrium olivine to the bulk-rock composition, allowing generation of potential parental melt compositions (Herzberg et al., 2007). Although accumulated olivines in typical picrites are out of equilibrium with the melts (e.g., Larsen and Pedersen, 2000; Li et al., 2012), the compositional differences between equilibrium olivine and accumulated olivine are small and negligible (Herzberg et al., 2007). About 3–8% olivines were subtracted from the bulk-rock for picritic lavas from Wulongba and Maoniuping. About 0–21% olivines were added in the bulk-rock for those from Tanglanghe and Wuguijing. The calculated major element compositions of the Emeishan primary magmas are listed in Table S3. The calculated MgO contents of primary magmas from Wulongba range from 18 to 19 wt%, which are slightly lower than those from Tanglanghe, Maoniuping and Wuguijing (MgO = 19–21 wt %). The calculated TiO₂ contents (~1.2 wt%) are lower, and Al₂O₃ contents (10.5–10.7 wt%) are higher for the primary melts from Wulongba, compared with those from Tanglanghe, Maoniuping and Wuguijing (TiO₂ = 1.5–2.0 wt%, Al₂O₃ = 7.9–10.0 wt%). All of the calculated primary melts display normal FeO_{Total} contents (11.1–11.9 wt %), exclude the possible existence of the late Permian ferropicritic magma (FeO_{Total} > 13 wt%, Hanski and Smolkin, 1995; Gibson et al., 2000) in the Lijiang-Dali region. The calculated primary magma compositions are generally similar to those of the most primitive melt inclusions hosted by olivine phenocrysts with high Fo contents (Fo > 91, Hanski et al., 2010). Estimation of trace element concentrations in primary magmas can simply be achieved by adding or subtracting olivine wherein the partition coefficients with respect to olivine are assumed to be zero. The concentrations of highly incompatible elements (e.g., Th, Nb, La, Ce) in primary melts from Wulongba are significantly lower than those from Tanglanghe, Maoniuping and Wuguijing (Table S3). In Fig. 7, Sm/Yb ratios are negatively correlated with Al₂O₃ contents and Na/Ti ratios for the Emeishan primary magmas.

It is difficult to determine the volatile contents (e.g., CO₂, H₂O) of the Emeishan primary magmas because continental lavas are generally degassed upon eruption. However, it has been observed that H₂O/Ce and CO₂/Nb keep nearly constant in MORB and in rare undegassed OIB basalts (Dixon et al., 2002; Saal et al., 2002; Cartigny et al., 2008).

$\text{H}_2\text{O}/\text{Ce}$ has been estimated to be about 200 (Dixon et al., 2002). CO_2/Nb has been estimated to be 239 and 530, respectively (Saal et al., 2002; Cartigny et al., 2008). The calculated Ce and Nb contents of the Emeishan primary magmas lead to estimate that the primary melts from Wulongba contain $\sim 0.24\%$ H_2O and $\sim 0.12\text{--}0.28\%$ CO_2 . The primary melts from Tanglanghe, Maoniuping and Wuguijing contain $\sim 0.7\text{--}1.2\%$ H_2O and $0.4\text{--}1.6\%$ CO_2 . The Emeishan primary melts are slightly poorer in volatile components compared with primary OIB ($\sim 0.2\text{--}1.6\text{ H}_2\text{O}$ and $\sim 0.1\text{--}3.0\text{ CO}_2$, Herzberg and Asimow, 2008). It is noted that Liu et al., (2017) reported that the H_2O content of the primary Dali picrite is about 3.44 wt%, which is significantly higher than those estimated in this study. Magma with such high H_2O content should crystallize hydrous minerals, such as hornblende and phlogopite. However, no hydrous mineral has been observed in the Emeishan picrites (e.g., Hanski et al., 2004; Zhang et al., 2006; Li et al., 2010, 2012; Kamenetsky et al., 2012; Yu et al., 2017; Ren et al., 2017; Wu et al., 2018), which indicates that the Emeishan picritic lavas are poor in water. Moreover, CO_2 abundances of the Emeishan picritic lavas can also be estimated using their SiO_2 and CaO contents. Experimental results have shown that, compared to anhydrous peridotite, addition of CO_2 can generate partial melts at very low temperatures and low mass fractions with substantially lower SiO_2 and elevated CaO (Dasgupta et al., 2007). Many oceanic island basalts have low SiO_2 and high CaO due to low degree partial melting of carbonated peridotite (Dasgupta et al., 2007). In the diagram of SiO_2 versus CaO (Fig. 8), all of the Emeishan picrites plot in the field of partial melts of carbonate-free fertile peridotite (Walter, 1998; Herzberg, 2004, 2006). This indicates that the Emeishan picritic lavas are CO_2 -barren melts and may be derived from a carbonate-barren mantle source. It is noted that some Dongchuan high-Mg tephrites ($\text{MgO} > 8\text{ wt\%}$) plot in the field of partial melts of carbonate-bearing peridotite.

5.3. The redox states and melting conditions of the Emeishan primary magmas

Vanadium can occur in various oxidation states (V^{2+} , V^{3+} , V^{4+} and V^{5+}) in silicate and oxide systems at terrestrial oxygen fugacities

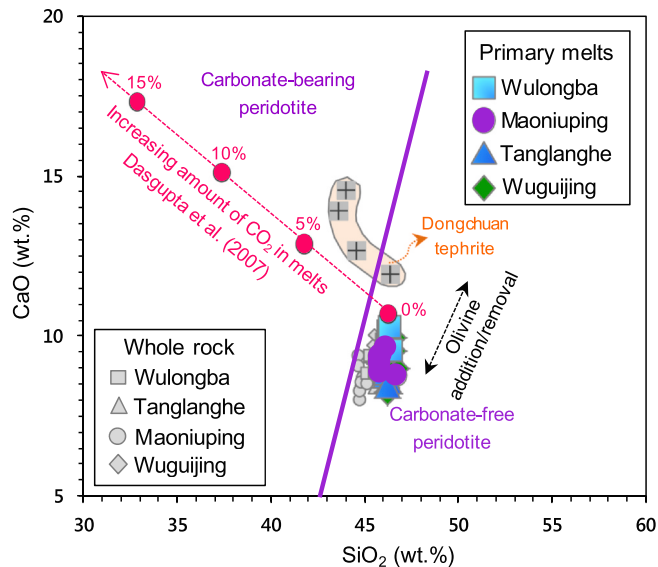


Fig. 8. CaO and SiO_2 contents of primary magmas of carbonate-bearing (Dasgupta et al., 2007) and carbonate-free fertile peridotite (Walter, 1998; Herzberg, 2004, 2006). The green line is an approximate filter that separates CO_2 -enriched and deficient lavas (after Herzberg and Asimow, 2008). Dongchuan Mg-rich tephrites ($\text{MgO} > 8\text{ wt\%}$) are also shown for comparison (Song et al., 2008b; Tian et al., 2017). (For interpretation of the references to colour in this figure legend, the reader is referred to the web version of this article.)

(Canil, 1997; Mallmann and O'Neill, 2009). Previous experimental studies demonstrated that partitioning behavior of V in the process of mantle melting and magma crystallization is dominantly controlled by the oxygen fugacity and is much less sensitive to the temperature and melt composition (Canil, 1997; Mallmann and O'Neill, 2009, 2013). As the partition coefficients of V between olivine and melt ($D_{\text{V}}^{\text{ol/melt}}$) under variable redox conditions were well determined (Mallmann and O'Neill, 2009, 2013), $D_{\text{V}}^{\text{ol/melt}}$ becomes an intuitive oxybarometer of magmas. Here we use the $D_{\text{V}}^{\text{ol/melt}}$ oxybarometer of Mallmann and O'Neill, (2013) to estimate the oxygen fugacities of the Emeishan picrites. Trace element data of olivine phenocrysts and whole rock for the Emeishan picrites used for calculation are from Yao et al., (2019) and Yu et al., (2017). The $D_{\text{V}}^{\text{ol/melt}}$ oxybarometer yields $\log f\text{O}_2$ of QFM for Wulongba, QFM + 0~+0.5 for Tanglanghe, Maoniuping and Wuguijing. The values are comparable to those of MORB (QFM + 0.1, Berry et al., 2018). To examine the reliability of the inferred results from the $D_{\text{V}}^{\text{ol/melt}}$ oxybarometer, the redox states of these picritic lavas were also evaluated independently from their whole-rock V/Sc and V/Ga ratios (Mallmann and O'Neill, 2009). The Wulongba picrites have average V/Sc and V/Ga of 8.6 ± 0.4 (1σ , $n = 7$) and 18.3 ± 1.7 (1σ , $n = 7$), respectively. The picritic lavas from Tanglanghe, Maoniuping and Wuguijing have average V/Sc and V/Ga of 7.1 ± 1.5 (1σ , $n = 7$) and 16.9 ± 2.6 (1σ , $n = 33$), respectively. These values are comparable to the modeled ratios for batch melting of peridotitic mantle at $\log f\text{O}_2$ of QFM (V/Sc = 8.5–10.2, V/Ga = 17.5–19.5, Mallmann and O'Neill, 2009). These results demonstrated that there is no clear difference in redox state for the Emeishan picritic lavas from different locations.

Mantle potential temperature (T_p) represents the assumed temperature that mantle may have supposing that it was adiabatically decompressed to surface without melting (McKenzie and Bickle, 1988). T_p information can be obtained by comparison of primary melt compositions with melt compositions determined from forward models of peridotite melting (Herzberg and Asimow, 2008). The calculated T_p values using PRIMELT3 range from 1516 to 1539 °C for primary melts from Wulongba, and from 1535 to 1596 °C for those from Tanglanghe, Maoniuping and Wuguijing (Fig. 9). The estimated T_p values in this study are similar with those estimated by Xu et al., (2001) (1500 ~ 1550 °C), but are slightly lower than those estimated by Zhang et al., (2006) and Li et al., (2012) (1590–1680 °C). In addition, mantle

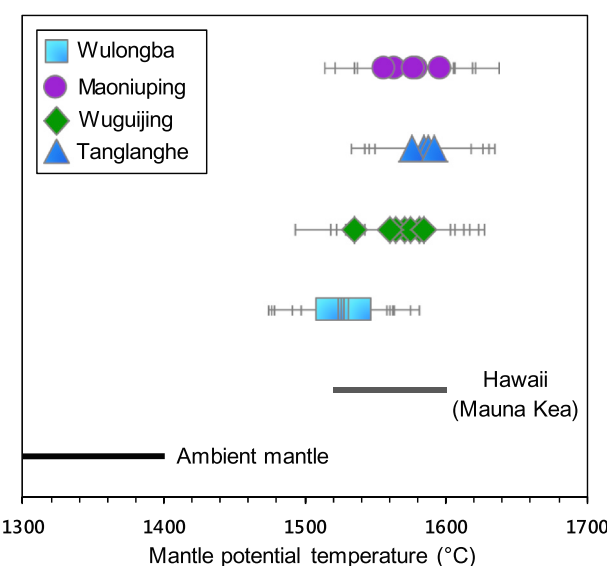


Fig. 9. Mantle potential temperature calculated using primary melts of the Emeishan picrites (after Herzberg and Asimow, 2015). The uncertainty is less than ± 42 °C. The ranges of mantle potential temperature of Hawaii plume and ambient mantle are after Herzberg and Gazel, (2009).

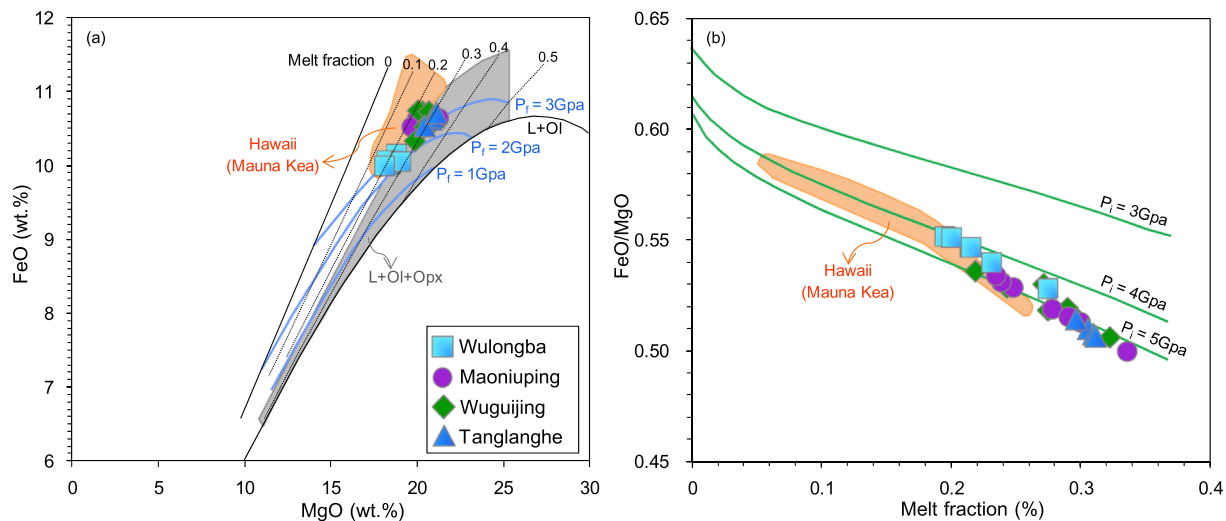


Fig. 10. (a) MgO versus FeO for the Emeishan primary melts. Blue contours are final melting pressure. Grey field are melts equilibrated with olivine and orthopyroxene (Herzberg and Asimow, 2015). Black dashed lines are melt fractions. (b) Melt fraction versus FeO/MgO, green contours are initial melting pressure. Pressures of initial and final melting are parameterizations of experimental data (Walter, 1998; Herzberg and O'Hara, 2002; Herzberg, 2004). The orange fields are primitive melts from Mauna Kea, Hawaii (Herzberg and Asimow, 2008). (For interpretation of the references to colour in this figure legend, the reader is referred to the web version of this article.)

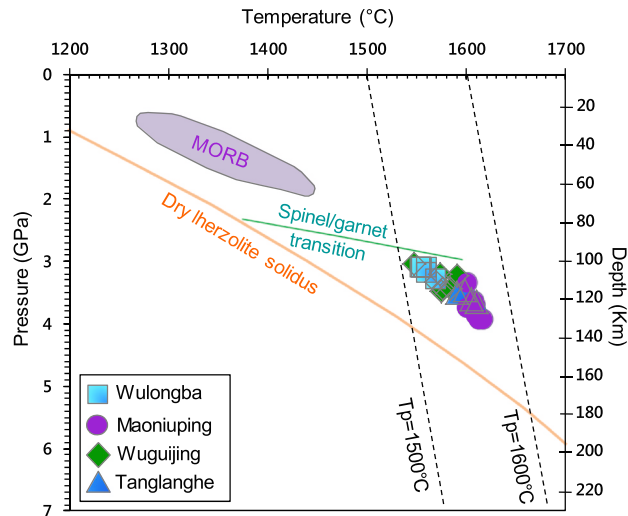


Fig. 11. Average melting pressure and temperature for the Emeishan picrites. The calculation method, peridotite solidus and the field of MORB are after Lee et al., (2009). The green line shows the phase transition between spinel and garnet peridotite (after Klemme and O'Neill, 2000). (For interpretation of the references to colour in this figure legend, the reader is referred to the web version of this article.)

potential temperatures of the Emeishan lavas are similar to those from Hawaii, and are about 200 °C higher than the average ambient mantle temperature (1350 °C, Herzberg et al., 2007), supporting the popular “hot plume” model for the Emeishan large igneous province (e.g., Xu et al., 2001; Xiao et al., 2004; Zhang et al., 2006). Low degree melting of mantle peridotite generates melt droplets which are efficiently removed from the residue by buoyancy-driven draining. These melt droplets mix to produce an “aggregate” or accumulated fractional melt during decompression melting (Hole and Millett, 2016). The melt fraction is uniquely defined by the MgO and FeO contents of any accumulated fractional melt (Herzberg and Asimow, 2008). FeO and MgO contents and melt fractions of the Emeishan primary magmas calculated using model PRIMELT3 are shown in Fig. 10. The melt fraction ranges from 0.19 to 0.27 for primary magmas from Wulongba, and from

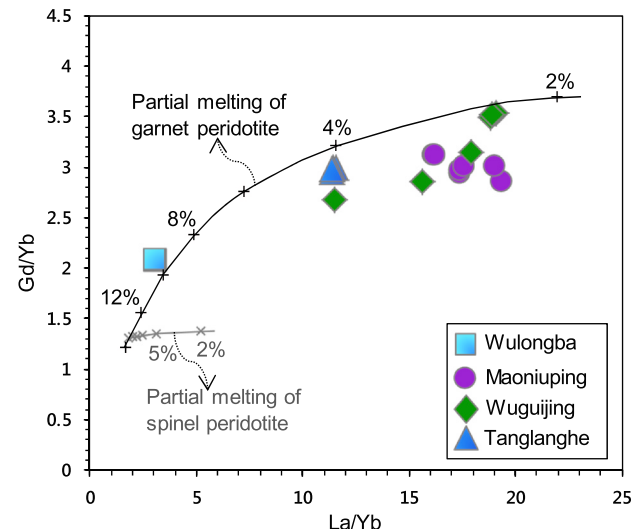


Fig. 12. Variations of bulk rock La/Yb and Gd/Yb ratios for the Emeishan picrites. The black curve represents the calculated melts after batch melting of the primitive garnet peridotite. The grey curve represents the calculated melts after batch melting of the primitive spinel peridotite. Mineral/melt partition coefficients, minerals proportions, melting mode are from Stracke et al., (2003). Numbers besides the curves represent variable degrees of partial melting. La, Yb and Gd concentrations of the primitive mantle are from Sun and McDonough (1989).

0.22 to 0.34 for those from Tanglanghe, Maoniuping and Wuguijing. In general, melt fractions for Emeishan are larger than those for Hawaii (0.05 to 0.25, Herzberg and Asimow, 2008). The high melt fractions, high mantle temperatures and large-scale magmatism related to the ELIP are all consistent with formation in mantle plume head.

Lee et al., (2009) provided a magma thermobarometer to calculate the average pressure and temperature of melt segregation from the mantle. The calculated results demonstrated that the primary magmas from Wulongba segregated at a shallower depth than those from other regions (Fig. 11). In addition, melting at high pressure will generate melts with high Sm/Yb, low Na/Ti and Al₂O₃ contents (e.g., Putirka, 1999; Walter, 1998). In Fig. 7, Sm/Yb ratios are negatively correlated with Al₂O₃ contents and Na/Ti ratios for the Emeishan primary

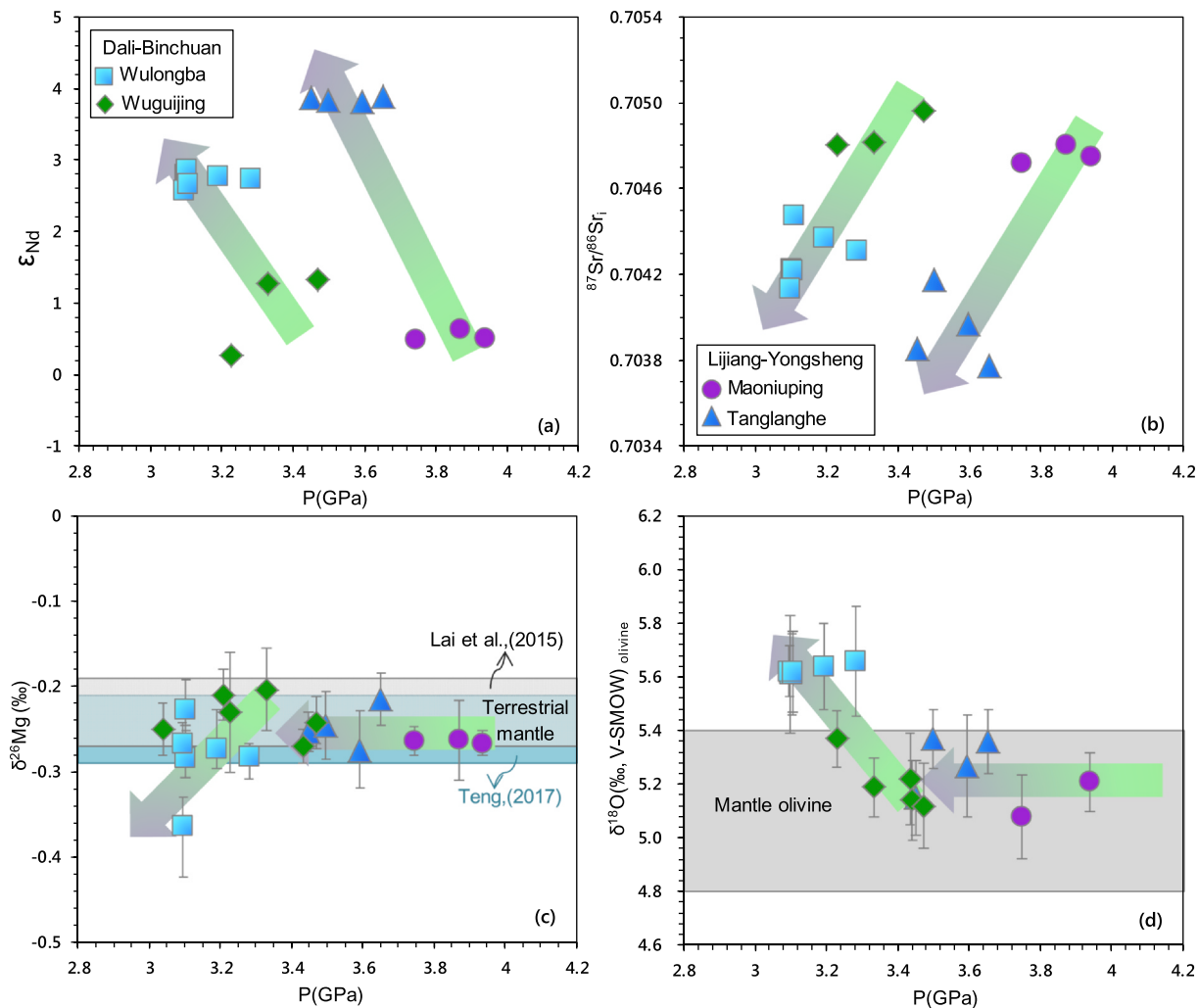


Fig. 13. Calculated mean melting pressure versus $^{87}\text{Sr}/^{86}\text{Sr}_i$ (a), $^{87}\text{Sr}/^{86}\text{Sr}_i$ (b), $\delta^{26}\text{Mg}$ (c) and $\delta^{18}\text{O}$ (d) for the Emeishan picritic lavas. Mean melting pressures are calculated using the software from Lee et al. (2009). The gray and light green bands represent recommended $\delta^{26}\text{Mg}$ values of the terrestrial mantle from Lai et al. (2015) and Teng, (2017), respectively. Oxygen isotope compositions of mantle olivine (4.8–5.4‰) are after Matthey et al., (1994). (For interpretation of the references to colour in this figure legend, the reader is referred to the web version of this article.)

magmas. The Wulongba picrites characterized by low Sm/Yb, high Na/Ti and Al₂O₃ can be attributed to partial melting at low pressure. In contrast, samples from Tanglanghe, Maoniuping and Wuguijing have high Sm/Yb, low Na/Ti and Al₂O₃, which can be explained by melting of peridotite at high pressure. Relationships between La/Yb and Gd/Yb also have been used by a number of researchers to determine “deep” (high pressure) versus “shallow” (low pressure) melting of peridotitic mantle for the Emeishan lavas (e.g., Xu et al., 2001; Xiao et al., 2004; Song et al., 2009). Low degree partial melting of deep garnet peridotite will generate melts with high Gd/Yb and La/Yb. High degree melting of shallow spinel peridotite will produce melts with low Gd/Yb and La/Yb (Fig. 12). Lavas from Tanglanghe, Maoniuping and Wuguijing have relatively high Gd/Yb and La/Yb, which may be entirely produced in the garnet stability field of the upper mantle. On the other hand, the Wulongba lavas with lower Gd/Yb and La/Yb roughly can be explained by melting of a peridotitic upper mantle in garnet-spinel transition zone.

In specific, decompression melting starts at some initial pressure (P_i) and ends at a final pressure which is usually determined by some boundary like the lithosphere-asthenosphere boundary. As shown in Fig. 10, pressures of final and initial melting represented by blue and green contours, respectively, are parameterizations of experimental data (Walter, 1998; Herzberg and O’Hara, 2002; Herzberg, 2004;

Herzberg et al., 2007). Melting begins at slightly lower pressures for the Wulongba lavas (~4 GPa) compared with those for the Tanglanghe, Maoniuping and Wuguijing lavas (~5 GPa, Fig. 10b). Melting always begins shallower when the source is cooler (Herzberg and Asimow, 2008). This is consistent with the slightly lower mantle potential temperatures for the Wulongba lavas (Fig. 9). The final melting pressures for the Wulongba lavas range from 2 to 3 Gpa (~70–100 km depth), which are lower than those for the Tanglanghe, Maoniuping and Wuguijing lavas (> 3 GPa, Fig. 10a). This suggests that the Wulongba lavas were generated in the garnet-spinel transition zone of the upper mantle. The Tanglanghe, Maoniuping and Wuguijing lavas were entirely generated in the garnet stability field of the upper mantle. If the estimated final melting pressure represents the depth of lithosphere-asthenosphere boundary, this indicates that lithosphere below Wulongba is thinner than that beneath other three areas. It is reasonable considering that Wulongba locates at the very edge of the western Yangtze Block (Figs. 1, 2). Previous studies considered that extension could have occurred at the margin of the western Yangtze Block, which rifting and opening of the Ganze-Litang Ocean that separated the Zhongza micro-block from the Yangtze Block (Chung and Jahn, 1995; Zhong, 1998). The lithosphere at the margin of the western Yangtze Block is expected to be thinned during extension.

5.4. Vertical stratification to isotopic heterogeneity in the mantle source

To test the possible vertical distribution of isotopic heterogeneity in the mantle, both radiogenic and stable isotopes for the Emeishan picrites are examined (Fig. 13). As shown in Fig. 2, the Wulongba and Wuguijing picrites occurred in the Dali-Binchuan volcanic field. The Maoniuping and Tanglanghe picrites occurred in the Lijiang-Yongsheng volcanic field. In the Dali-Binchuan volcanic field, lavas produced at shallower level of the mantle tend to have higher ϵ_{Nd} and lower $^{87}\text{Sr}/^{86}\text{Sr}_i$ than those produced at depth. In the Lijiang-Yongsheng volcanic field, lavas produced at shallower level of the mantle also tend to have higher ϵ_{Nd} and lower $^{87}\text{Sr}/^{86}\text{Sr}_i$ than those produced at depth. This suggests the mantle sources for lavas from both the Dali-Binchuan and Lijiang-Yongsheng volcanic fields are vertically stratified in Sr-Nd isotopic compositions. However, the situation is different for the stable isotopic compositions of the Emeishan lavas. For example, in the Lijiang-Yongsheng volcanic field, lavas derived from mantle at depth display similar normal $\delta^{26}\text{Mg}$ and $\delta^{18}\text{O}$ values with those produced at shallower level of the mantle. In contrast, in the Dali-Binchuan volcanic field, lavas produced at shallower level of the mantle tend to have slightly lower $\delta^{26}\text{Mg}$ and higher $\delta^{18}\text{O}$ values compared with those produced at depth. This suggests only shallower mantle beneath Dali-Binchuan contains recycled sedimentary carbonates (magnesite).

6. Conclusion

The picrites from Maoniuping, Tanglanghe and Wuguijing exhibit typical OIB-like trace element patterns, depleted Sr-Nd isotopic compositions ($^{87}\text{Sr}/^{86}\text{Sr}_i = 0.7038\text{--}0.7050$; $\epsilon_{\text{Nd}} = 0.27\text{--}3.89$), normal mantle-like $\delta^{26}\text{Mg}$ (-0.27 to -0.2%) and $\delta^{18}\text{O}$ ($5.0\text{--}5.4\text{\textperthousand}$), which can be explained by partial melting of plume source materials with negligible sedimentary carbonates. The Wulongba picrites are characterized by flat trace element patterns, depleted Sr-Nd isotopic compositions ($^{87}\text{Sr}/^{86}\text{Sr}_i = 0.7041\text{--}0.7045$; $\epsilon_{\text{Nd}} = 2.57\text{--}2.85$), slightly lower $\delta^{26}\text{Mg}$ (-0.36 to $-0.23\text{\textperthousand}$) and higher $\delta^{18}\text{O}$ (5.6 to $5.7\text{\textperthousand}$), which were attributed to involvement of minor sedimentary carbonates (magnesite) in their mantle source. The calculated mantle potential temperatures using PRIMELT3 software range from 1516 to $1539\text{ }^{\circ}\text{C}$ for primary melts from Wulongba, and from 1535 to $1596\text{ }^{\circ}\text{C}$ for those from Tanglanghe, Maoniuping and Wuguijing. Melting begins at slightly lower pressures for the Wulongba picrites ($\sim 4\text{ GPa}$) compared with those of the Tanglanghe, Maoniuping and Wuguijing picrites ($\sim 5\text{ GPa}$). The final melting pressures for the Wulongba lavas range from 2 to 3 Gpa , which are lower than those for the Tanglanghe, Maoniuping and Wuguijing lavas ($> 3\text{ GPa}$). This suggests that the Wulongba lavas were generated in shallower garnet-spinel transition zone of the upper mantle. The Tanglanghe, Maoniuping and Wuguijing lavas were entirely generated in the garnet stability field of the upper mantle.

CRediT authorship contribution statement

Song-Yue Yu: Conceptualization, Writing - original draft. **Lie-Meng Chen:** Writing - review & editing. **Jiang-Bo Lan:** Software, Methodology. **Yong-Sheng He:** Data curation, Formal analysis. **Qi Chen:** Data curation, Formal analysis. **Xie-Yan Song:** Supervision, Project administration.

Declaration of Competing Interest

The authors declare that they have no known competing financial interests or personal relationships that could have appeared to influence the work reported in this paper.

Acknowledgments

This study was funded by the National Key R & D Program of China (2016YFC0600502), the strategic priority research program (B) of the Chinese Academy of Sciences (XDB18000000), Key Special Project for Introduced Talents Team of Southern Marine Science and Engineering Guangdong Laboratory (Guangzhou) (GML2019ZD0202), NSFC (41573009, 41873026), “Western Light Young scholar” program of Chinese Academy of Sciences. We greatly appreciate constructive comments from Professor Zhao-Chong Zhang and the other two anonymous reviewers.

Appendix A. Supplementary material

Supplementary data to this article can be found online at <https://doi.org/10.1016/j.jseas.2020.104534>.

References

- Ali, J.R., Thompson, G.M., Zhou, M.-F., Song, X., 2005. Emeishan large igneous province, SW China. *Lithos* 79, 475–489.
- An, Y., Wu, F., Xiang, Y., Nan, X., Yu, X., Yang, J., Yu, H., Xie, L., Huang, F., 2014. High-precision Mg isotope analyses of low-Mg rocks by MC-ICP-MS. *Chem. Geol.* 390, 9–21.
- Arndt, N.T., Czamanske, G.K., Wooden, J.L., Fedorenko, V.A., 1993. Mantle and crustal contributions to continental flood volcanism. *Tectonophysics* 223, 39–52.
- Arndt, N.T., Christensen, U., 1992. The role of lithospheric mantle in continental flood volcanism: Thermal and geochemical constraints. *J. Geophys. Res.* 97, 10967.
- Baker, J.A., Macpherson, C.G., Menzies, M.A., Thirlwall, M.F., Al-Kadasi, M., Mattey, D.P., 2000. Resolving crustal and mantle contributions to continental flood Volcanism, Yemen; constraints from mineral oxygen isotope data. *J. Petrol.* 41, 1805–1820.
- Berry, A.J., Stewart, G.A., O'Neill, H.S.C., Mallmann, G., Mosselmans, J.F.W., 2018. A reassessment of the oxidation state of iron in MORB glasses. *Earth Planet. Sci. Lett.* 483, 114–123.
- Brenot, A., Cloquet, C., Vigier, N., Carignan, J., France-Lanord, C., 2008. Magnesium isotope systematics of the lithologically varied Moselle river basin, France. *Geochim. Cosmochim. Acta* 72, 5070–5089.
- Canil, D., 1997. Vanadium partitioning and the oxidation state of Archaean komatiite magmas. *Nature* 389, 842–845.
- Carlson, R.W., 1991. Physical and chemical evidence on the cause and source characteristics of flood basalt volcanism. *Aust. J. Earth Sci.* 38, 525–544.
- Cartigny, P., Pineau, F., Aubaud, C., Javoy, M., 2008. Towards a consistent mantle carbon flux estimate: Insights from volatile systematics (H₂O/Ce, 8D, CO₂/Nb) in the North Atlantic mantle (14° N and 34° N). *Earth Planet. Sci. Lett.* 265, 672–685.
- Cheng, Z., Zhang, Z., Hou, T., Santosh, M., Chen, L., Ke, S., Xu, L., 2017. Decoupling of Mg-C and Sr-Nd-O isotopes traces the role of recycled carbon in magnesiocarbonates from the Tarim Large Igneous Province. *Geochim. Cosmochim. Acta* 202, 159–178.
- Cheng, Z., Zhang, Z., Xie, Q., Hou, T., Ke, S., 2018. Subducted slab-plume interaction traced by magnesium isotopes in the northern margin of the Tarim Large Igneous Province. *Earth Planet. Sci. Lett.* 489, 100–110.
- Chung, S.-L., Jahn, B.-M., 1995. Plume-lithosphere interaction in generation of the Emeishan flood basalts at the Permian-Triassic boundary. *Geology* 23, 889–892.
- Courtier, A.M., Jackson, M.G., Lawrence, J.F., Wang, Z., Lee, C.-T.A., Halama, R., Warren, J.M., Workman, R., Xu, W., Hirschmann, M.M., Larson, A.M., Hart, S.R., Lithgow-Bertelli, C., Stixrude, L., Chen, W.-P., 2007. Correlation of seismic and petrologic thermometers suggests deep thermal anomalies beneath hotspots. *Earth Planet. Sci. Lett.* 264, 308–316.
- Dasgupta, R., Hirschmann, M.M., Smith, N.D., 2007. Partial Melting Experiments of Peridotite + CO₂ at 3 GPa and Genesis of Alkaline Ocean Island Basalts. *J. Petrol.* 48, 2093–2124.
- Deniel, C., Pin, C., 2001. Single-stage method for the simultaneous isolation of lead and strontium from silicate samples for isotopic measurements. *Anal. Chim. Acta* 426, 95–103.
- Depaolo, D.J., 1981. Trace-element and isotopic effects of combined wallrock assimilation and fractional crystallization. *Earth Planet. Sci. Lett.* 53, 189–202.
- Depaolo, D.J., 1986. Detailed record of the neogene-Sr isotopic evolution of seawater from DSDP Site-590B. *Geology* 14, 103–106.
- Dixon, J.E., Leist, L., Langmuir, C., Schilling, J.G., 2002. Recycled dehydrated lithosphere observed in plume-influenced mid-ocean-ridge basalt. *Nature* 420, 385–389.
- Galy, A., Bar-Matthews, M., Halicz, L., O'Nions, R.K., 2002. Mg isotopic composition of carbonate: insight from speleothem formation. *Earth Planet. Sci. Lett.* 201, 105–115.
- Gibson, S., Thompson, R., Dickin, A., 2000. Ferropicrites: geochemical evidence for Fe-rich streaks in upwelling mantle plumes. *Earth Planet. Sci. Lett.* 174, 355–374.
- Guo, B.-J., Zhu, X.-K., Dong, A.-G., Yan, B., Shi, G.-H., Zhao, Z., 2019. Mg isotopic systematics and geochemical applications: A critical review. *J. Asian Earth Sci.* 176, 368–385.
- Hanski, E., Kamenetsky, V.S., Luo, Z.-Y., Xu, Y.-G., Kuzmin, D.V., 2010. Primitive magmas in the Emeishan Large Igneous Province, southwestern China and northern Vietnam.

- Lithos 119, 75–90.
- Hanski, E., Walker, R.J., Huhma, H., Polyakov, G.V., Balykin, P.A., Hoa, T.T., Phuong, N.T., 2004. Origin of the Permian-Triassic komatiites, northwestern Vietnam. *Contrib. Miner. Petrol.* 147, 453–469.
- Hanski, E., Smolkin, V., 1995. Iron-and LREE-enriched mantle source for early Proterozoic intraplate magmatism as exemplified by the Pechenga ferropicrites, Kola Peninsula, Russia. *Lithos* 34, 107–125.
- Hawkesworth, C.J., Rogers, N.W., van Calsteren, P.W.C., Menzies, M.A., 1984. Mantle enrichment processes. *Nature* 311, 331–335.
- He, Q., Xiao, L., Balta, B., Gao, R., Chen, J., 2010. Variety and complexity of the Late-Permian Emeishan basalts: reappraisal of plume-lithosphere interaction processes. *Lithos* 119, 91–107.
- He, B., Xu, Y.-G., Chung, S.-L., Xiao, L., Wang, Y., 2003. Sedimentary evidence for a rapid, kilometer-scale crustal doming prior to the eruption of the Emeishan flood basalts. *Earth Planet. Sci. Lett.* 213, 391–405.
- Hei, H.-X., Su, S.-G., Wang, Y., Mo, X.-X., Luo, Z.-H., Liu, W.-G., 2018. Rhyolites in the Emeishan large igneous province (SW China) with implications for plume-related felsic magmatism. *J. Asian Earth Sci.* 164, 344–365.
- Hergt, J.M., Peate, D.W., Hawkesworth, C.J., 1991. The petrogenesis of Mesozoic Gondwana low-Ti flood basalts. *Earth Planet. Sci. Lett.* 105, 134–148.
- Herzberg, C., Asimow, P.D., 2008. Petrology of some oceanic island basalts: PRIMELT2.XLS software for primary magma calculation. *Geochem. Geophys. Geosyst.* 9, Q09001.
- Herzberg, C., Asimow, P.D., 2015. PRIMELT3 MEGA.XLSM software for primary magma calculation: Peridotite primary magma MgO contents from the liquidus to the solidus. *Geochem. Geophys. Geosyst.* 16, 563–578.
- Herzberg, C., Gazel, E., 2009. Petrological evidence for secular cooling in mantle plumes. *Nature* 458, 619–622.
- Herzberg, C., O'Hara, M.J., 2002. Plume-Associated Ultramafic Magmas of Phanerozoic Age. *J. Petrol.* 43, 1857–1883.
- Herzberg, C., 2004. Geodynamic information in peridotite petrology. *J. Petrol.* 45, 2507–2530.
- Herzberg, C., 2006. Petrology and thermal structure of the Hawaiian plume from Mauna Kea volcano. *Nature* 444, 605–609.
- Herzberg, C., Asimow, P.D., Arndt, N., Niu, Y., Lesher, C.M., Fitton, J.G., Cheadle, M.J., Saunders, A.D., 2007. Temperatures in ambient mantle and plumes: Constraints from basalts, picrites, and komatiites. *Geochem. Geophys. Geosyst.* 8, Q02006.
- Higgins, J.A., Schrag, D.P., 2010. Constraining magnesium cycling in marine sediments using magnesium isotopes. *Geochim. Cosmochim. Acta* 74, 5039–5053.
- Hole, M.J., Millett, J.M., 2016. Controls of mantle potential temperature and lithospheric thickness on magmatism in the north atlantic igneous province. *J. Petrol.* 57, 417–436.
- Huang, J., Xiao, Y., 2016. Mg-Sr isotopes of low-826Mg basalts tracing recycled carbonate species: Implication for the initial melting depth of the carbonated mantle in Eastern China. *Int. Geol. Rev.* 58, 1350–1362.
- Huang, F., Zhang, Z., Lundstrom, C.C., Zhi, X., 2011. Iron and magnesium isotopic compositions of peridotite xenoliths from Eastern China. *Geochim. Cosmochim. Acta* 75, 3318–3334.
- Kamenetsky, V.S., Chung, S.-L., Kamenetsky, M.B., Kuzmin, D.V., 2012. Picrites from the Emeishan Large Igneous Province, SW China: a Compositional Continuum in Primitive Magmas and their Respective Mantle Sources. *J. Petrol.* 53, 2095–2113.
- Ke, S., Teng, F.-Z., Li, S.-G., Gao, T., Liu, S.-A., He, Y., Mo, X., 2016. Mg, Sr, and O isotope geochemistry of syenites from northwest Xinjiang, China: Tracing carbonate recycling during Tethyan oceanic subduction. *Chem. Geol.* 437, 109–119.
- Kinzler, R.J., Grove, T.L., 1992. Primary magmas of Mid-Ocean Ridge basalts. 2. Applications. *J. Geophys. Res.-Solid Earth* 97, 6907–6926.
- Kinzler, R.J., 1997. Melting of mantle peridotite at pressures approaching the spinel to garnet transition: Application to Mid-Ocean Ridge basalt petrogenesis. *J. Geophys. Res.-Solid Earth* 102, 853–874.
- Klein, E.M., Langmuir, C.H., 1987. Global correlations of ocean ridge basalt chemistry with axial depth and crustal thickness. *J. Geophys. Res.-Solid Earth Planets* 92, 8089–8115.
- Klemme, S., O'Neill, H.S.C., 2000. The near-solidus transition from garnet Iherzolite to spinel Iherzolite. *Contrib. Miner. Petrol.* 138, 237–248.
- Kushiro, I., 1975. Nature of silicate melt and its significance in magma genesis – regularities in shift of liquidus boundaries involving olivine, pyroxene, and silica minerals. *Am. J. Sci.* 275, 411–431.
- Larsen, L.M., Pedersen, A.K., 2000. Processes in high-Mg, high-T magmas: Evidence from olivine, chromite and glass in Paleocene picrites from West Greenland. *J. Petrol.* 41, 1071–1098.
- Lai, Y.-J., Pogge von Strandmann, P.A.E., Dohmen, R., Takazawa, E., Elliott, T., 2015. The influence of melt infiltration on the Li and Mg isotopic composition of the Horoman Peridotite Massif. *Geochim. Cosmochim. Acta* 164, 318–332.
- Le Bas, M., 2000. IUGS reclassification of the high-Mg and picritic volcanic rocks. *J. Petrol.* 41, 1467–1470.
- Lee, C.-T.A., Luffi, P., Plank, T., Dalton, H., Leeman, W.P., 2009. Constraints on the depths and temperatures of basaltic magma generation on Earth and other terrestrial planets using new thermobarometers for mafic magmas. *Earth Planet. Sci. Lett.* 279, 20–33.
- Li, C., Tao, Y., Qi, L., Ripley, E.M., 2012. Controls on PGE fractionation in the Emeishan picrites and basalts: Constraints from integrated lithophile–siderophile elements and Sr-Nd isotopes. *Geochim. Cosmochim. Acta* 90, 12–32.
- Li, C., Ripley, E.M., Tao, Y., Hu, R., 2016. The significance of PGE variations with Sr-Nd isotopes and lithophile elements in the Emeishan flood basalts province from SW China to northern Vietnam. *Lithos* 248, 1–11.
- Li, J., Xu, J.-F., Suzuki, K., He, B., Xu, Y.-G., Ren, Z.-Y., 2010. Os, Nd and Sr isotope and trace element geochemistry of the Muli picrites: Insights into the mantle source of the Emeishan Large Igneous Province. *Lithos* 119, 108–122.
- Liu, J., Xia, Q.-K., Kuritani, T., Hanski, E., Yu, H.-R., 2017. Mantle hydration and the role of water in the generation of large igneous provinces. *Nat. Commun.* 8, 1824.
- Liu, S.A., Teng, F.Z., Yang, W., Wu, F.Y., 2011. High-temperature inter-mineral magnesium isotope fractionation in mantle xenoliths from the North China craton. *Earth Planet. Sci. Lett.* 308, 131–140.
- Mallmann, G., O'Neill, H.S.C., 2013. Calibration of an empirical thermometer and oxygen barometer based on the partitioning of Sc, Y and V between olivine and silicate melt. *J. Petrol.* 54, 933–949.
- Mallmann, G., O'Neill, H.S.C., 2009. The crystal/melt partitioning of V during mantle melting as a function of oxygen fugacity compared with some other elements (Al, P, Ca, Sc, Ti, Cr, Fe, Ga, Y, Zr and Nb). *J. Petrol.* 50, 1765–1794.
- Mattey, D., Lowry, D., Macpherson, C., 1994. Oxygen isotope composition of mantle peridotite. *Earth Planet. Sci. Lett.* 128, 231–241.
- McKenzie, D., Bickle, M.J., 1988. The volume and composition of melt generated by extension of the lithosphere. *J. Petrol.* 29, 625–679.
- Miková, J., Denková, P., 2007. Modified chromatographic separation scheme for Sr and Nd isotope analysis in geological silicate samples. *J. Geosci.* 52, 221–226.
- Norman, M.D., Garcia, M.O., 1999. Primitive magmas and source characteristics of the Hawaiian plume: petrology and geochemistry of shield picrites. *Earth Planet. Sci. Lett.* 168, 27–44.
- Pin, C., Zalduegui, J.S., 1997. Sequential separation of light rare-earth elements, thorium and uranium by miniaturized extraction chromatography: Application to isotopic analyses of silicate rocks. *Anal. Chim. Acta* 339, 79–89.
- Plank, T., Langmuir, C.H., 1998. The chemical composition of subducting sediment and its consequences for the crust and mantle. *Chem. Geol.* 145, 325–394.
- Pogge von Strandmann, P.A.E., Burton, K.W., James, R.H., van Calsteren, P., Gislason, S.R., Sigfusson, B., 2008. The influence of weathering processes on riverine magnesium isotopes in a basaltic terrain. *Earth Planet. Sci. Lett.* 276, 187–197.
- Putirka, K.D., 1999. Melting depths and mantle heterogeneity beneath Hawaii and the East Pacific Rise: Constraints from Na/Ti and rare earth element ratios. *J. Geophys. Res.-Solid Earth* 104, 2817–2829.
- Putirka, K.D., 2008. Thermometers and barometers for volcanic systems. In: Putirka, K.D., Tepley, F.J., III (Eds.), Minerals, Inclusions and Volcanic Processes. Mineralogical Society of America and Geochemical Society, Reviews in Mineralogy and Petrology 69, 61–120.
- Putirka, K.D., Perfit, M., Ryerson, F.J., Jackson, M.G., 2007. Ambient and excess mantle temperatures, olivine thermometry, and active vs. passive upwelling. *Chem. Geol.* 241, 177–206.
- Ren, Z.-Y., Wu, Y.-D., Zhang, L., Nichols, A.R.L., Hong, L.-B., Zhang, Y.-H., Zhang, Y., Liu, J.-Q., Xu, Y.-G., 2017. Primary magmas and mantle sources of Emeishan basalts constrained from major element, trace element and Pb isotope compositions of olivine-hosted melt inclusions. *Geochim. Cosmochim. Acta* 208, 63–85.
- Rudnick, R.L., Fountain, D.M., 1995. Nature and composition of the continental crust: a lower crustal perspective. *Rev. Geophys.* 33, 267–309.
- Saal, A.E., Hauri, E.H., Langmuir, C.H., Perfit, M.R., 2002. Vapour undersaturation in primitive mid-ocean-ridge basalt and the volatile content of Earth's upper mantle. *Nature* 419, 451–455.
- Schauble, E.A., 2011. First-principles estimates of equilibrium magnesium isotope fractionation in silicate, oxide, carbonate and hexaaquamagnesium(2+) crystals. *Geochim. Cosmochim. Acta* 75, 844–869.
- Shellnutt, J.G., Zhou, M.-F., 2007. Permian peralkaline, peraluminous and metaluminous A-type granites in the Panxi district, SW China: Their relationship to the Emeishan mantle plume. *Chem. Geol.* 243, 286–316.
- Song, X.-Y., Keays, R.R., Xiao, L., Qi, H.-W., Ihlenfeld, C., 2009. Platinum-group element geochemistry of the continental flood basalts in the central Emeishan Large Igneous Province, SW China. *Chem. Geol.* 262, 246–261.
- Song, X.-Y., Zhou, M.-F., Tao, Y., Xiao, J.-F., 2008a. Controls on the metal compositions of magmatic sulfide deposits in the Emeishan large igneous province, SW China. *Chem. Geol.* 253, 38–49.
- Song, X.-Y., Qi, H.-W., Robinson, P.T., Zhou, M.-F., Cao, Z.-M., Chen, L.-M., 2008b. Melting of the subcontinental lithospheric mantle by the Emeishan mantle plume: evidence from the basal alkaline basalts in Dongchuan, Yunnan, Southwestern China. *Lithos* 100, 93–111.
- Song, X.-Y., Zhou, M.-F., Hou, Z.-Q., Cao, Z.-M., Wang, Y.-L., Li, Y., 2001. Geochemical constraints on the mantle source of the upper Permian Emeishan continental flood basalts, southwestern China. *Int. Geol. Rev.* 43, 213–225.
- Stracke, A., Biziatis, M., Salters, V.J.M., 2003. Recycling oceanic crust: Quantitative constraints. *Geochim. Geophys. Geosyst.* 4, 8003.
- Su, B.X., Hu, Y., Teng, F.Z., Qin, K.Z., Yang, B., Sakyi, P.A., Tang, D.M., 2017. Chromite-induced magnesium isotope fractionation during mafic magma differentiation. *Sci. Bull.* 62, 1538–1546.
- Su, B.-X., Hu, Y., Teng, F.-Z., Xiao, Y., Zhang, H.-F., Sun, Y., Bai, Y., Zhu, B., Zhou, X.-H., Ying, J.-F., 2019. Light Mg isotopes in mantle-derived lavas caused by chromite crystallization, instead of carbonatite metasomatism. *Earth Planet. Sci. Lett.* 522, 79–86.
- Sun, S.S., McDonough, W.F., 1989. Chemical and isotopic systematics of oceanic basalts: implications for mantle composition and processes. In: Saunders, A.D., Norry, M.J. (Eds.), Magmatism in the Ocean Basins. Geological Society Special Publication, 42, pp. 313–345.
- Tanaka, T., Togashi, S., Kamioka, H., Amakawa, H., Kagami, H., Hamamoto, T., Yuhara, M., Orihashi, Y., Yoneda, S., Shimizu, H., 2000. JNdI-1: a neodymium isotopic reference in consistency with LaJolla neodymium. *Chem. Geol.* 168, 279–281.
- Teng, F.Z., 2017. Magnesium isotope geochemistry. *Rev. Mineral. Geochem.* 82, 219–287.
- Teng, F.-Z., Li, W.-Y., Ke, S., Yang, W., Liu, S.-A., Sedaghatpour, F., Wang, S.-J., Huang, K.-J., Hu, Y., Ling, M.-X., Xiao, Y., Liu, X.-M., Li, X.-W., Gu, H.-O., Sio, C.K., Wallace,

- D.A., Su, B.-X., Zhao, L., Chamberlin, J., Harrington, M., Brewer, A., 2015. Magnesium isotopic compositions of international geological reference materials. *Geostand. Geoanal. Res.* 39, 329–339.
- Teng, F.-Z., Li, W.-Y., Ke, S., Marty, B., Dauphas, N., Huang, S., Wu, F.-Y., Pourmand, A., 2010. Magnesium isotopic composition of the Earth and chondrites. *Geochim. Cosmochim. Acta* 74, 4150–4166.
- Teng, F.-Z., Wadhwa, M., Helz, R.T., 2007. Investigation of magnesium isotope fractionation during basalt differentiation: Implications for a chondritic composition of the terrestrial mantle. *Earth Planet. Sci. Lett.* 261, 84–92.
- Tian, H.-C., Yang, W., Li, S.-G., Ke, S., 2017. Could sedimentary carbonates be recycled into the lower mantle? Constraints from Mg isotopic composition of Emeishan basalts. *Lithos* 292–293, 250–261.
- Tipper, E.T., Galy, A., Bickle, M.J., 2006. Riverine evidence for a fractionated reservoir of Ca and Mg on the continents: Implications for the oceanic Ca cycle. *Earth Planet. Sci. Lett.* 247, 267–279.
- Walter, M.J., 1998. Melting of garnet peridotite and the origin of komatiite and depleted lithosphere. *J. Petrol.* 39, 29–60.
- Wang, X.J., Chen, L.H., Hofmann, A.W., Hanyu, T., Kawabata, H., Zhong, Y., Xie, L.W., Shi, J.H., Miyazaki, T., Hirahara, Y., Takahashi, T., Senda, R., Chang, Q., Vaglarov, B.S., Kimura, J.I., 2018. Recycled ancient ghost carbonate in the Pitcairn mantle plume. *PNAS* 115, 8682–8687.
- White, R.S., McKenzie, D., 1995. Mantle plumes and flood basalts. *J. Geophys. Res. Solid Earth* 100, 17543–17585.
- Wu, Y.-D., Ren, Z.-Y., Handler, M.R., Zhang, L., Qian, S.-P., Xu, Y.-G., Wang, C.-Y., Wang, Y., Chen, L.-L., 2018. Melt diversity and magmatic evolution in the dali picrites, Emeishan large igneous province. *J. Geophys. Res. Solid Earth* 123, 9635–9657.
- Xiao, L., Xu, Y.-G., Mei, H.-J., Zheng, Y.-F., He, B., Pirajno, F., 2004. Distinct mantle sources of low-Ti and high-Ti basalts from the western Emeishan large igneous province, SW China: implications for plume-lithosphere interaction. *Earth Planet. Sci. Lett.* 228, 525–546.
- Xu, Y., Chung, S.-L., Jahn, B.-M., Wu, G., 2001. Petrologic and geochemical constraints on the petrogenesis of Permian-Triassic Emeishan flood basalts in southwestern China. *Lithos* 58, 145–168.
- Xu, Y.-G., Chung, S.-L., Shao, H., He, B., 2010. Silicic magmas from the Emeishan large igneous province, Southwest China: Petrogenesis and their link with the end-Guadalupian biological crisis. *Lithos* 119, 47–60.
- Yang, C., Liu, S.A., 2019. Zinc isotope constraints on recycled oceanic crust in the mantle sources of the Emeishan large igneous province. *J. Geophys. Res. Solid Earth* 124, 12537–12555.
- Yao, J.-H., Zhu, W.-G., Li, C., Zhong, H., Yu, S., Ripley, E.M., Bai, Z.-J., 2019. Olivine O isotope and trace element constraints on source variation of picrites in the Emeishan flood basalt province, SW China. *Lithos* 338–339, 87–98.
- Young, E.D., Galy, A., 2004. The isotope geochemistry and cosmochemistry of magnesium. *Rev. Mineral. Geochem.* 55, 197–230.
- Young, E.D., Tonui, E., Manning, C.E., Schauble, E., Macris, C.A., 2009. Spinel-olivine magnesium isotope thermometry in the mantle and implications for the Mg isotopic composition of Earth. *Earth Planet. Sci. Lett.* 288, 524–533.
- Yunnan, 1990. Regional geology of Yunnan province. Geological Memoirs, Series, 21. Geologic Press, Beijing (in Chinese).
- Yu, S.-Y., Shen, N.-P., Song, X.-Y., Ripley, E.M., Li, C., Chen, L.-M., 2017. An integrated chemical and oxygen isotopic study of primitive olivine grains in picrites from the Emeishan Large Igneous Province, SW China: Evidence for oxygen isotope heterogeneity in mantle sources. *Geochim. Cosmochim. Acta* 215, 263–276.
- Yu, S.-Y., Xu, Y.-G., Huang, X.-L., Ma, J.-L., Ge, W.-C., Zhang, H.-H., Qin, X.-F., 2009. Hf-Nd isotopic decoupling in continental mantle lithosphere beneath Northeast China: Effects of pervasive mantle metasomatism. *J. Asian Earth Sci.* 35, 554–570.
- Zhang, Z., Mahoney, J.J., Mao, J., Wang, F., 2006. Geochemistry of picritic and associated basalt flows of the western Emeishan Flood Basalt Province, China. *J. Petrol.* 47, 1997–2019.
- Zhang, Z., Zhi, X., Chen, L., Saunders, A.D., Reichow, M.K., 2008. Re-Os isotopic compositions of picrites from the Emeishan flood basalt province, China. *Earth Planet. Sci. Lett.* 276, 30–39.
- Zhang, L., Ren, Z.-Y., Handler, M.R., Wu, Y.-D., Zhang, L., Qian, S.-P., Xia, X.-P., Yang, Q., Xu, Y.-G., 2019. The origins of high-Ti and low-Ti magmas in large igneous provinces, insights from melt inclusion trace elements and Sr-Pb isotopes in the Emeishan Large Igneous Province. *Lithos* 344–345, 122–133.
- Zhong, D.L., 1998. The Paleo-Tethys Orogen in Western of Yunnan and Sichuan. Science Press, Beijing (in Chinese).
- Zhong, Y., Chen, L.-H., Wang, X.-J., Zhang, G.-L., Xie, L.-W., Zeng, G., 2017. Magnesium isotopic variation of oceanic island basalts generated by partial melting and crustal recycling. *Earth Planet. Sci. Lett.* 463, 127–135.
- Zhou, M.-F., Arndt, N.T., Malpas, J., Wang, C.Y., Kennedy, A.K., 2008. Two magma series and associated ore deposit types in the Permian Emeishan large igneous province, SW China. *Lithos* 103, 352–368.